applied sciences

MDPI

Article

PLA-Based Films Reinforced with Cellulose Nanofibres from *Salicornia ramosissima* By-Product with Proof of Concept in High-Pressure Processing

Alexandre R. Lima [1,2,3], Nathana L. Cristofoli [1], Inès Delahousse [4], Renata A. Amaral [2], Jorge A. Saraiva [2] and Margarida C. Vieira [1,5,*]

1 MED—Mediterranean Institute for Agriculture, Environment and Development & CHANGE—Global Change and Sustainability Institute, Faculty of Sciences and Technology, Campus de Gambelas, Universidade do Algarve, 8005-139 Faro, Portugal; alexandrelima@greencolab.com (A.R.L.); nlcristofoli@ualg.pt (N.L.C.)
2 LAQV–REQUIMTE—Associated Laboratory for Green Chemistry of the Network of Chemistry and Technology, Department of Chemistry, Universidade de Aveiro, 3810-193 Aveiro, Portugal; a.renatal.amaral@gmail.pt (R.A.A.); jorgesaraiva@ua.pt (J.A.S.)
3 GreenCoLab—Associação Oceano Verde, Universidade do Algarve, 8005-139 Faro, Portugal
4 L'Institut Agro Dijon, Université Bourgogne Franche Comté, 26 Bd Docteur Petitjean—BP 87999, 21079 Dijon, France; ines.delahousse@live.fr
5 ISE—High Institute of Engineering, Department of Food Engineering, Campus da Penha, Universidade do Algarve, 8000-139 Faro, Portugal
* Correspondence: mvieira@ualg.pt

Featured Application

This study developed sustainable biocomposite films of polylactic acid (PLA) reinforced with cellulose nanofibres (CNFs) from *Salicornia ramosissima* by-products for food packaging. Solvent-cast films exhibited excellent flexibility, transparency, and moisture resistance, while electrospun films demonstrated higher tensile strength and rigidity. The CNF-reinforced PLA kept its integrity under high-pressure processing, confirming its industrial feasibility. Overall, the PLA/CNF biocomposites present a promising, environmentally responsible alternative for next-generation sustainable packaging, aligned with circular economy strategies and sustainable development goals.

Abstract

Biocomposite films based on polylactic acid (PLA) reinforced with cellulose nanofibers (CNFs) extracted from *Salicornia ramosissima* by-products were developed and characterised using solvent casting (SC) and electrospinning (ES) techniques. The primary objective was to assess their suitability as sustainable food packaging materials that are compatible with high-pressure processing (HPP). The SC films exhibited a transparent, homogeneous morphology with superior ductility and water vapour barrier performance, whereas the ES films displayed a fibrous, porous structure with enhanced tensile strength and rigidity. The incorporation of CNFs significantly improved the mechanical properties, particularly the tensile strength and Young's modulus, with optimal reinforcement achieved at a loading of 0.5%. Thermal and spectroscopic analyses confirmed the effective integration of CNF without compromising the thermal stability of PLA. Pouch-type packages from CNF-reinforced SC films withstood industrial HPP conditions without rupture or leakage, demonstrating their technical feasibility for food packaging applications. This study presents the first demonstration of *Salicornia ramosissima* by-product valorisation for CNF production and its application in HPP-compatible food packaging, addressing both circular economy goals and emerging food processing technologies.

check for updates

Academic Editor: Adem Gharsallaoui

Received: 21 October 2025
Revised: 6 December 2025
Accepted: 8 December 2025
Published: 18 December 2025

Citation: Lima, A.R.; Cristofoli, N.L.; Delahousse, I.; Amaral, R.A.; Saraiva, J.A.; Vieira, M.C. PLA-Based Films Reinforced with Cellulose Nanofibres from *Salicornia ramosissima* By-Product with Proof of Concept in High-Pressure Processing. *Appl. Sci.* **2025**, *15*, 13247. https://doi.org/10.3390/app152413247

Keywords: biobased films; polylactic acid; cellulose nanofibers; food packaging; solvent casting; electrospinning; high-pressure processing

1. Introduction

The balance between food safety and environmental sustainability is a crucial dilemma for the food industry. The European Union's Packaging and Packaging Waste Regulation mandates a reduction in single-use plastics, limits packaging volume, and sets targets for recycled content (30% by 2030) [1]. In parallel, the Sustainable Development Goals (SDGs) of the 2030 Agenda reinforce the necessity for circular models, with a strong emphasis on reverse logistics and waste minimisation [2]. However, sustainable materials, such as those based on cellulose or biopolymers, often present technical challenges, including lower resistance to moisture and oxygen, which can compromise microbiological safety and the shelf life of food products [3,4]. These regulatory and technical demands urgently require innovation in both the materials and the manufacturing processes.

Utilising agro-industrial residues to produce cellulose nanofibers (CNFs) has emerged as a strategy aligned with circular economy principles. Several studies have demonstrated that organic waste and byproducts can be used to produce cellulose nanofibers [5–8]. Several nanofibers often have high crystallinity and Young's moduli, as well as the ability to reinforce polymer matrices and improve the mechanical and barrier properties of biodegradable films [9–11]. Furthermore, their inclusion can reduce water vapour permeability, a critical factor for food packaging applications [9,12,13]. The utilisation of a by-product from Salicornia, a halophyte plant abundant in coastal regions, adds value to an otherwise underutilised by-product, reducing both costs and the environmental impact associated with its disposal [6].

Polylactic acid (PLA), derived from renewable sources such as cornstarch and sugarcane, proves to be a promising alternative to conventional plastics. Its production emits less CO_2 compared to fossil-based polymers, and its biodegradability under controlled conditions makes it ideal for short-term applications [14–17]. The global PLA market is expected to grow at a compound annual growth rate (CAGR) of over 20% through 2030, driven by the rising demand for biodegradable plastic packaging [18]. Low thermal resistance, melting strength, high brittleness, and low flexibility restrict its broader use [19]. The addition of CNF is a viable solution to these drawbacks. PLA/CNF composites exhibit an increase in elastic modulus and improved dimensional stability, enabling their application in flexible films and thermoformed containers [20,21].

Solvent casting and electrospinning are two promising methods for producing CNF-reinforced films. Both methods are scalable; electrospinning is already used industrially to produce filters, textiles, and medical materials [22], while solvent casting can be adapted to continuous coating lines [23]. Solvent casting, widely used at the laboratory scale, involves the homogeneous dispersion of CNF in polymer solutions, followed by controlled drying [24]. Despite its simplicity, this method faces challenges, including bubble formation and prolonged evaporation times. In contrast, electrospinning technology enables the production of continuous nanofibers (50–500 nm in diameter) through the application of electric fields, creating porous structures with high surface area [25–27]. In the packaging sector, films produced by electrospinning stand out due to enhanced mechanical properties, protective functionalities, and controlled permeability, turning them promising for advanced solutions [28–30]. Future development prospects for this technology include the adoption of multi-nozzle or needleless systems, biodegradable and recycled polymers, and addressing environmental and health challenges related to the kind of solvent

used and nanofiber disposal [31,32]. Furthermore, research is focused on creating new nanocomposites and functional coatings for smart packaging applications [33,34].

High-Pressure Processing (HPP) is a non-thermal food preservation technology that subjects usually pre-packaged foods, but not only these, to isostatic pressures ranging from 400 to 600 MPa, typically for an abbreviated time [35,36]. In response to consumer demand for additive-free and minimally thermally processed foods, HPP offers vegetative microbial safety and significantly extends shelf life while preserving the freshness, taste, and nutritional value of food products, claiming to be a clean-label trend [37–39]. Notably, food products are processed in their final packaging, which minimises the risk of recontamination after the preservation process and requires flexible packaging (either flasks, pouches or bottles). For food safety and environmental reasons, the development of sustainable non-plastic packaging materials compatible with high-pressure conditions has become increasingly important as HPP adoption grows.

This study aimed to evaluate the reinforcing effect of CNF extracted from *Salicornia ramosissima* by-product in a PLA-based biocomposite film across two distinct processing techniques (solvent casting and electrospinning). Each technique was optimised according to its specific technical requirements and pouch-type food packaging. The experimental framework encompassed: (1) production of CNF-reinforced films (0.5–1% CNF loading) via solvent casting and electrospinning; (2) comparative evaluation of physicochemical, optical, mechanical, thermal, and structural properties; and (3) proof-of-concept testing of the food packaging under HPP conditions. The results validated the technical feasibility of these biocomposites and established critical parameters for industrial-scale production, thereby advancing the development of packaging solutions aligned with the Sustainable Development Goals (SDGs) and emerging legislative frameworks.

2. Materials and Methods

2.1. Cellulose Nanofibres

Cellulose nanofibres (CNFs) from the agro-industrial by-product of Salicornia (parts of stems and roots) were produced on a laboratory scale from the extraction of cellulose, followed by the nanofibres' isolation by a proposed enzymatic treatment, as described in detail in our previous study [6]. In this process, nanocellulose was isolated from cellulose (previously extracted from plant residues) by sequentially using cellulase and xylanase (Megazyme, Bray, Ireland). The complete hydrolysis of cellulose relies on the synergistic action of these two enzymes within the cellulase complex (Endoglucanase, exoglucanase and β-glucosidase). The CNF used in this study had previously been morphologically and structurally characterised [6], exhibiting an average diameter of 18–25 nm (TEM analysis), length distribution of 200–800 nm, aspect ratio (L/D) of 20–45, crystallinity index of 68% (XRD), and specific surface area of 45–60 m^2 g^{-1}. The D/L lactide ratio is not applicable here, as CNFs are cellulose-based rather than polylactic acid-based; instead, their high aspect ratio and crystallinity are the key features underpinning their reinforcing potential in polymer matrices.

2.2. PLA-Based Films and Processing Techniques

Optimisation of the polymer concentrations was performed for each technique: 2% (*w*/*v*) for SC to ensure proper film formation with controlled solvent evaporation and 10% (*w*/*v*) for ES to achieve adequate solution viscosity for continuous fibre formation. These concentrations represent the established protocols for each processing method and reflect the technical requirements inherent to SC and ES techniques.

This study represents an initial proof of concept using laboratory-scale techniques to evaluate the reinforcing potential of CNF in PLA-based films. For industrial-scale produc-

tion, there is a need to implement solvent-free methods to meet food safety regulations (e.g., melt extrusion) or green solvents (e.g., ethanol and ethyl acetate) with closed-loop solvent recovery systems.

2.2.1. Solvent Casting (SC)

Suspensions of CNF at concentrations of 0.5 and 1 wt.% were dissolved in 100 mL of 99% pure chloroform (Sigma-Aldrich, St. Louis, MO, USA) by stirring each solution continuously for 30 min using a magnetic stirrer (ARE, VELP Scientifica, Usmate Velate, Italy) at room temperature (RT, 25 ± 1 °C) until a stable CNF colloidal suspension was obtained, with no visible sedimentation during film forming. The solutions were then filtered through a cheesecloth to remove any dispersed insoluble impurities. PLA biopolymer granules 3–5 mm in diameter (∅) with a natural colour, biodegradable properties, and a molecular weight of 230 kg mol^{-1} were obtained from Goodfellow Cambridge Ltd. (Huntingdon, England). The PLA granules were used as received without further purification, and PLA 2% (*w*/*v*) was added to each chloroform/CNF solution. After stirring continuously at RT for 60 min, or until the PLA granules were fully dissolved, 25 mL of the film-forming solution was cast onto circular glass plates (∅ = 90 mm). The plates were placed in a fume hood for 24 h to allow complete solvent evaporation and film drying. Control films were prepared using chloroform 99% and PLA (without CNF). Figure 1 presents the detailed scheme of PLA-based film production by the solvent casting method.

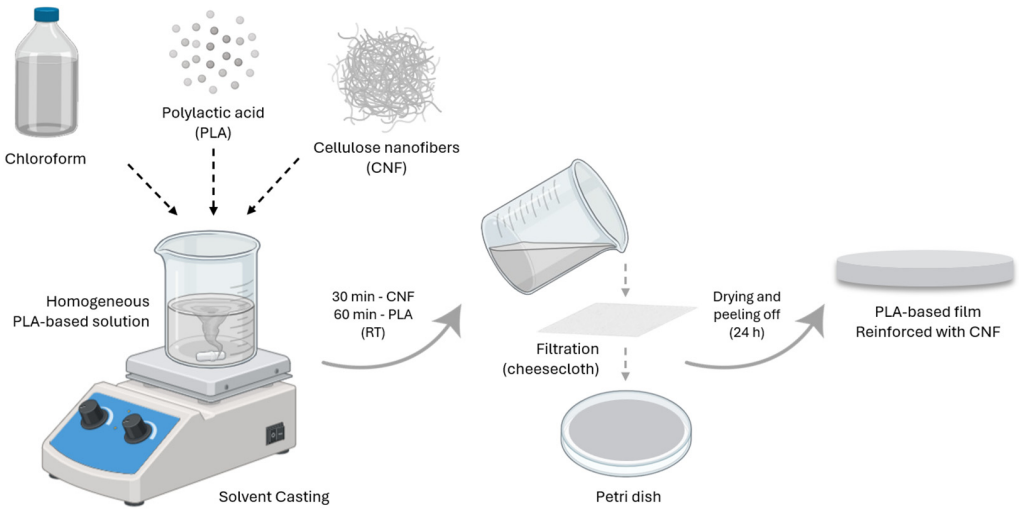

Figure 1. Scheme of PLA-based film production by solvent casting technique.

2.2.2. Electrospinning (ES)

The PLA-based films reinforced with CNF were prepared using an electrospinning unit (NanoSpinner Starter Kit, Inovenso Inc., Cambridge, MA, USA) equipped with a flat collector (7000 Series Aluminium Alloy, Stainless Steel) and integrated with a single-syringe micro-pump system (Inovenso Inc., Cambridge, MA, USA). The equipment operated at 0–30 kV, with a voltage precision of 0.1 kV and a maximum current of 0.170 mA.

Polymeric solutions (control) were prepared by dissolving 10% (*w*/*v*) PLA in chloroform (ISO-stabilised with ethanol for analysis) and stirring the mixture for 90 min at room temperature (RT). Two mixtures of PLA + CNF were tested with 0.5 and 1 wt.% CNF. First, CNF was added to chloroform and stirred for 45 min at RT. To remove potential insoluble particles, the mixture was filtered through cheesecloth. As a final step, the mixture was filtered and PLA was added, followed by the same procedure as previously described for the control solution. In the electrospinning process, three polymer formulations were used:

neat PLA (control) and PLA with CNF blends at concentrations of 10%, 10% plus 0.5%, and 10% plus 1%. A stainless-steel syringe needle fitted with an industrial nozzle designed with a flat end (1.2 mm × 60 mm, 18 G) was connected to a 10 mL plastic monojet syringe (BD Emerald™, Franklin Lakes, NJ, USA), dispensing each polymer formulation as a thin fibre towards a grounded aluminium foil fixed to a flat collector positioned perpendicularly at 12 cm from the syringe tip, where the fibres were collected. A constant voltage of 10 kV was applied to all polymeric solutions, and the polymer flow rate was set to 1.0 mL h^{-1}. Figure 2 illustrates the system, which is composed of the electrospinning unit, flat collector, and operational setup.

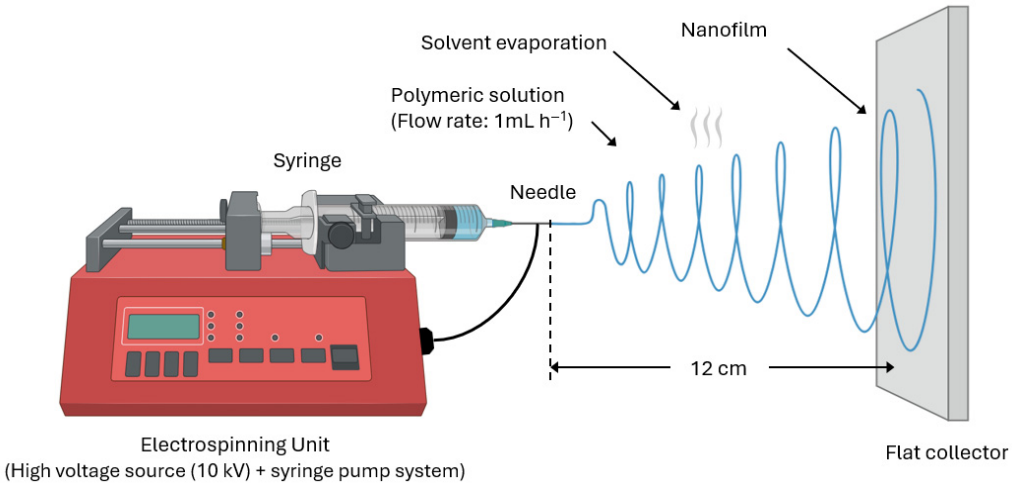

Figure 2. Graphical representation of the electrospinning process to obtain PLA-based films reinforced with cellulose nanofibers.

The obtained PLA-based films were placed in a fume hood for 24 h to eliminate any residual solvent and then stored in a desiccator until further analysis to prevent moisture absorption.

The experimental design is presented in Supplementary Table S1, where each experimental condition was prepared with at least three independent replicates (n = 3) for all analyses, thereby maintaining the 2 × 3 factorial design whenever possible.

2.3. Characterisation of Films

2.3.1. Colour and Opacity

Colour parameters and opacity measurements were performed using a PCE-CSM10 spectrophotometer calibrated with an EU-certified white standard tile (L^* = 84.67, a^* = −0.55, b^* = −0.68). The CIE Lab system quantifies colour through three parameters: L^* represents luminosity (0 for black to 100 for white), a^* indicates the green–red axis (negative to positive values), and b^* represents the blue–yellow axis (negative to positive values). Measurements were performed at three distinct points on each film sample. The total colour difference (ΔE) was calculated using Equation (1).

$$\Delta E = (\Delta L^*)^2 + (\Delta a^*)^2 + ((\Delta b^*)^2)^{1/2} \quad (1)$$

2.3.2. Thickness and Mechanical Properties

The film thickness was measured using a bench micrometre (model MTS, Adamel Lhomargy MI2, Saint-Baldoph, France) at six random points across the surface of each sample.

A texture analyser (model CTX, AMETEK Brookfield, Middleborough, MA, USA) fitted with tensile grips was used to assess the mechanical properties following the ASTM

D882-18 standard protocol for thin plastic sheeting [40]. The film samples were prepared as strips measuring 80 mm in length and 10 mm in width, with an exposed testing area of 5 cm^2 and a constant crosshead speed of 0.5 mm s^{-1} during testing. The data were processed using the Texture Pro V 1.0 Build 19 software (AMETEK Brookfield, Middleborough, MA, USA). Young's modulus was calculated based on the linear portion of the stress–strain curves, while the tensile strength was estimated from the corresponding stress–strain curves.

$$E = \frac{\sigma}{\varepsilon} \quad (2)$$

In Equation (2), "E" is the Young's modulus, "σ" represents the applied force per unit area, and "ε" is the axial strain, which indicates the proportional deformation.

2.3.3. Moisture and Solubility in Aqueous Medium

Film samples were prepared as 4 cm^2 squares and analysed for moisture content and water solubility. The samples were weighed before and after drying at 105 °C for 24 h for moisture evaluation. The moisture content was calculated from the mass difference using Equation (3), where *Mi* and *Mf* represent the initial and final masses, respectively.

$$M\ (\%) = \frac{M_i - M_f}{M_i} 100 \quad (3)$$

The water solubility was assessed using the dried specimens (*Mi*) from moisture analysis by immersing them in deionised water (50 mL) and keeping them at room temperature (25 °C) with gentle agitation for 7 days. After filtering the remaining insoluble portions, they were oven-dried (105 °C, 24 h), cooled in a desiccator for 30 min, and weighed (*Mf*). The percentage of soluble matter was determined using Equation (4). A triplicate of every measurement was taken.

$$Water\ Solubility\ (\%) = \frac{M_i - M_f}{M_i} 100 \quad (4)$$

2.3.4. Water Vapour Permeability (*WVP*)

Water Vapour Permeability (*WVP*) was gravimetrically determined according to ASTM E96/E96M-15 standard method [41], based on the experiment conducted by de Farias et al. [42] with some adaptations, at 25 ± 2 °C.

The PLA-based films reinforced with CNF, prepared via solvent casting and electrospinning, and their respective controls (without CNF) were all cut into circular shapes (Æ ≅ 35 mm). Glass permeation cells were dried in an oven for 24 h and weighed after cooling. Then, the cells were filled with 5 g of dried silica gel and sealed with the samples on top using silicone adhesive. The assembled cells were weighed using an analytical balance (ACS 200-4, Kern & Sohn, Balingen, Germany). To establish steady-state conditions, the cells were then placed in desiccators containing distilled water. Using an analytical scale, mass measurements were taken hourly for 9 h. The WVP was determined using Equation (5), where "x" represents the average film thickness, "A" is the film permeation area (9.62 × 10^{-4} m^2), "ΔP" is the partial pressure difference between the atmosphere above silica gel and pure water (3.168 kPa at 25 °C), and the term W/t represents the slope of the linear regression obtained from weight gain versus time data.

$$WVP = \frac{Wx}{tA\Delta P} \quad (5)$$

2.3.5. Water Contact Angle (WCA)

The hydrophilicity of the samples was characterised by the sessile drop method, measuring the water contact angle with the surfaces. The ambient temperature was set at 25.0 ± 0.1 °C. Water droplets with 4 ± 0.5 µL were generated using a micrometric syringe and deposited on the sample surfaces. Images were acquired using a video camera coupled to a microscope (Wild Herrbrugg M3Z Stereo Microscope, Leica Microsystems, Wetzlar, Germany) and a frame grabber (Data Translation DT3155) and then analysed using ADSA-P software (Axisymmetric Drop Shape Analysis Profile, Toronto, ON, Canada). The reported results are the mean of eight experiments.

2.3.6. Scanning Electron Microscopy (SEM)

Scanning electron microscopy (Hitachi TM4000, Ibaraki, Japan) was employed to examine the microstructure of solvent-cast and electrospun PLA-based films, both with and without CNF reinforcement. Samples were placed on aluminium stubs using double-sided carbon adhesive tape and observed at an accelerating voltage of 5 kV. The tests were conducted in triplicate for each sample, with an actual region size of 30 µm and a magnification of 1000×.

2.3.7. Thermogravimetry Analysis (TGA)

Thermal stability of the PLA-based films reinforced with CNF and produced by solvent casting and electrospinning was evaluated by thermogravimetric analysis following the standard protocol [43]. Measurements were conducted on a NETZSCH STA 449 F3 Jupiter® simultaneous thermal analyser (Selb, Bavaria, Germany). Samples (10–45 mg) were heated in Al2O3 crucibles from 30 °C to 700 °C at a rate of 10 °C min^{-1} under a controlled atmosphere. The system employed argon as the protective gas (20 mL min^{-1}) and nitrogen as the purge gas (50 mL min^{-1}). Film degradation temperatures were determined by identifying the onset of mass variation and the lowest temperature at which the mass loss process concluded.

2.3.8. Attenuated Total Reflectance–Fourier Transformed Infrared (ATR-FTIR)

Infrared spectra were obtained using a Nicolet 5700 micro-FTIR spectrophotometer (Thermo Fisher Scientific, Waltham, MA, USA) with attenuated total reflectance (ATR). Measurements were recorded in the wavelength range of 250,000 to 50 cm^{-1} (visible to far-infrared) using diffuse and ATR reflection modes. Each spectrum comprised 128 scans at 4 cm^{-1} resolution, with data processing performed via OMNIC Spectra software, v9.13, (Thermo Fisher Scientific, Waltham, MA, USA).

2.4. Food Packaging

The "pouch-type" packages were made from PLA-based film sheets, and after removal from the moulds, the films were cut into rectangular shapes (120 × 70 mm). Two identical parts were overlapped and heat-sealed on three sides using a benchtop vacuum sealer (Silvercrest®, Vaccum Packaging Machine, 125 W, Lidl Stiftung & Co. KG., Neckarsulm, Germany). After sealing, the packages were finished by removing excess film beyond the sealed boundaries. In the final version, the packages had rectangular dimensions of 100 × 50 mm.

2.5. High-Pressure Processing (HPP)

High-Pressure Processing (HPP) was used for the packaging proof-of-concept tests with a pilot-scale Hyperbaric Model 55 unit, a 55 L vessel with 2000 mm length and 200 mm diameter (Burgos, Spain). HPP testing was conducted exclusively on SC films due to their superior ductility (41.8–48.8% elongation at break), lower water vapour permeability

($0.07 \times 10^{-10} \pm 0.01 \times 10^{-10}$ g·m^{-2}·s^{-1}·Pa^{-1}), and transparent homogeneous morphology, essential characteristics for flexible food packaging applications. Even though ES films exhibited higher tensile strength, their brittle behaviour (6.89–7.71% elongation) and porous structure were unsuitable for liquid containment under isostatic pressure. Each pouch-type package was filled with fresh *Salicornia ramosissima* (1 g) and distilled water (15 mL) and heat-sealed. Subsequently, as these were initial validation tests, the samples were placed inside rectangular PA/PE (85 microns) pouches (150 × 100 mm) suitable for HPP processing. This precautionary measure was implemented to prevent sample leakage into the equipment if the PLA-based packaging failed. Furthermore, this procedure did not interfere with packaging validation, nor did it reduce or avoid the applied pressure load. A total of 18 packages (six samples in triplicate) were processed simultaneously in a single batch at standard conditions of 500 MPa for 5 min at 25 °C (typical conditions for HPP commercial pasteurisation). Post-processing visual inspection was conducted to evaluate package integrity, specifically examining for ruptures and liquid leakage.

2.6. Statistical Analysis

The results are presented as the mean ± standard deviation (SD) based on at least three replicates. To identify statistically significant differences between the films for each parameter, we performed a one-way analysis of variance (ANOVA) followed by Tukey's Honestly Significant Difference (HSD) test. The significance level was set at 5% ($p < 0.05$). Statistical analyses were conducted using Statistica 7.0 software (Statsoft Inc., Tulsa, OK, USA).

3. Results

3.1. Optical Properties

The visual assessment of all films, both those produced by solvent casting (SC) and electrospinning (ES) techniques, revealed homogeneous films without visible surface roughness (Figure 3). This result was achieved due to pre-filtration after CNF incorporation in the mixture for both production methods, as well as the good solubility of the PLA, chloroform, and CNF mixture. However, solvent-cast films (control, 0.5 and 1 wt.%) exhibited the excellent transparency characteristics of conventional films currently available in the plastics market, both PLA-based and those made from other polymers. The electrospun films displayed a white/opaque appearance with some translucency, although the longitudinal wave patterns on the back side of the paper could still be discerned with some difficulty, as shown in Figure 3. Due to the porous three-dimensional network and higher film thickness, the electrospun films produced more air–fibre interfaces, resulting in increased light scattering and higher opacity values, which were further intensified by CNF inclusions. This aspect was similar to that reported by Liu et al. [44] for electrospun PLA-based films with tea polyphenol nanofibers for food packaging applications.

In this case, SC films demonstrated low opacity, approximately 8%, with no significant difference between the control sample and CNF-reinforced samples. Meanwhile, ES films showed opacity values of 37.0% and 37.2% for control-ES and CNF05-ES samples, respectively, with a significant increase to 42.2% for the CNF1-ES sample (Table 1).

This opacity difference between films made from the same materials (PLA, chloroform, and CNF) but using different techniques can be attributed to their microstructural morphology. Electrospun films are formed by a network of misaligned, heterogeneous microfibres [45,46]. Furthermore, the rapid solvent evaporation and fibre stretching due to the applied electric field (10 kV) do not allow sufficient time for polymer chain reorganisation [47,48]. These individual fibres, combined with the fibrous structure, form a porous structure that causes multiple light scattering through the material, resulting in the white/opaque appearance. In contrast, films produced by SC undergo slow solvent evapo-

ration, allowing polymer chains time to reorganise and form a continuous, homogeneous structure, resulting in transparent films.

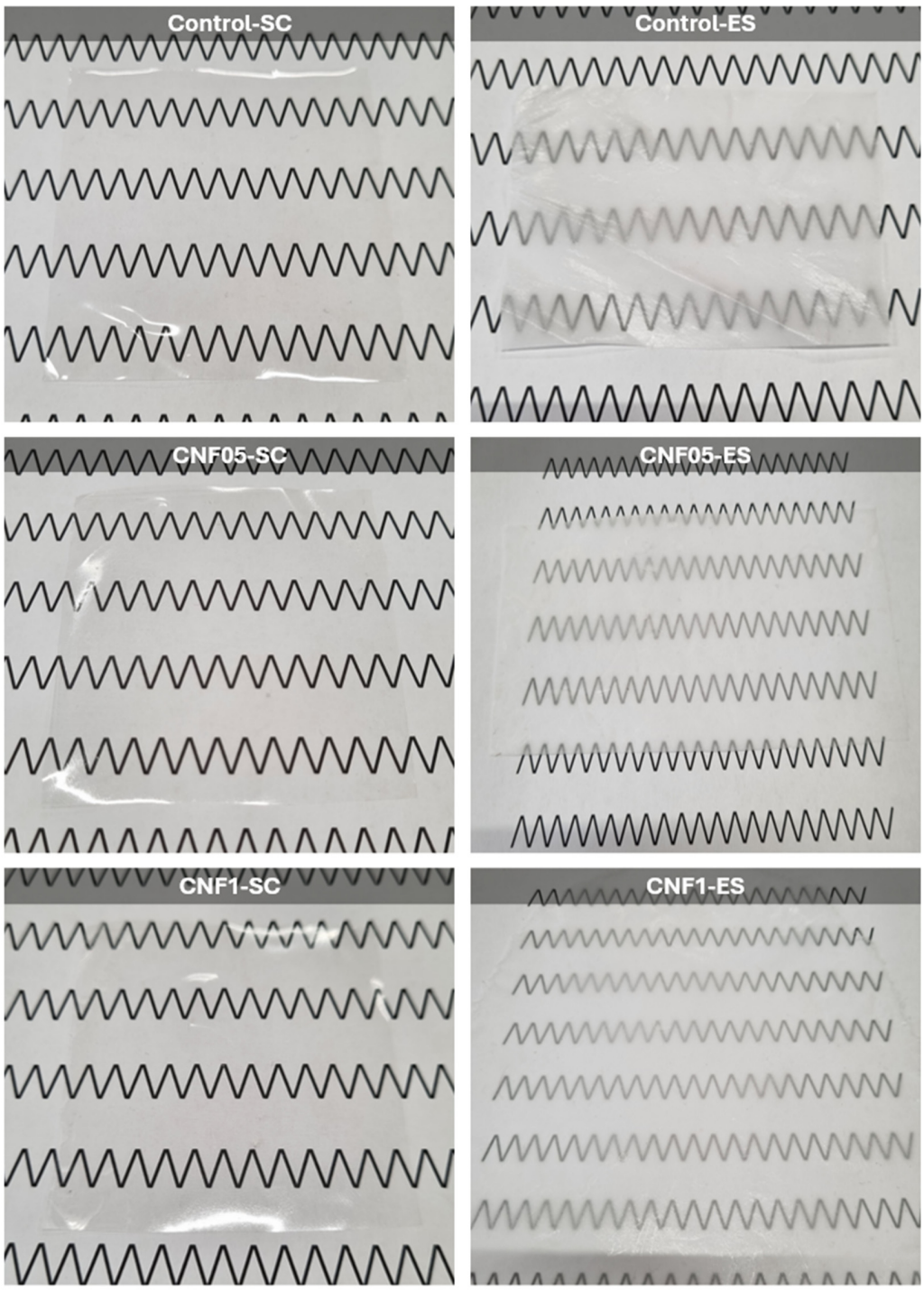

Figure 3. Visual aspect of PLA-based films reinforced with CNF by solvent casting (SC) and electrospinning (ES) techniques, with respective controls (without CNF), with paper with longitudinal wave patterns on the back side to better ascertain transparency.

Regarding colour, PLA-based films produced by electrospinning exhibited significantly higher luminosity values than solvent-cast films, as expressed by the L^* parameter. This result indicates a lighter/whiter appearance of electrospun samples and correlates with the previously discussed opacity differences, where the fibrous microstructure of electrospun films caused more light scattering, resulting in a whiter appearance [19].

In this case, with 68.7% luminosity, the sample with 1% CNF (CNF1-ES) was significantly higher than the others, suggesting that increased CNF content promotes a more fibrous microstructure formation in the films, resulting in stronger light scattering and a whiter, more opaque film. This is consistent with Sun et al. [49], who observed that nanofibril-rich films have enhanced light scattering and reduced transmittance due to their fibrous and porous structure, and with Xiao et al. [50], who highlighted that the electrospinning process increases reflection and scattering at air–fibre interfaces, producing brighter, more opaque membranes.

Table 1. Colour parameters and opacity of films.

Film	Opacity (%)	Colour			
		*L**	*a**	*b**	Δ*E**
Control-SC	7.98 ± 0.37 ^{a}	33.1 ± 0.14 ^{a}	−0.51 ± 0.04 ^{ab}	2.03 ± 0.08 ^{b}	
CNF05-SC	8.57 ± 0.09 ^{a}	33.4 ± 0.19 ^{a}	−0.52 ± 0.03 ^{ab}	1.82 ± 0.20 ^{b}	0.39 ^{a}
CNF1-SC	8.49 ± 0.12 ^{a}	33.5 ± 0.10 ^{a}	−0.51 ± 0.04 ^{ab}	1.78 ± 0.10 ^{b}	0.45 ^{a}
Control-ES	37.0 ± 1.32 ^{b}	54.1 ± 0.75 ^{b}	−0.38 ± 0.20 ^{a}	−1.42 ± 0.31 ^{a}	
1CNF05-ES	37.2 ± 1.02 ^{b}	55.8 ± 0.05 ^{b}	−0.80 ± 0.06 ^{a}	−1.30 ± 0.13 ^{a}	5.88 ^{b}
CNF1-ES	42.2 ± 2.80 ^{c}	68.7 ± 0.66 ^{c}	−0.46 ± 0.13 ^{a}	−1.08 ± 0.49 ^{a}	8.90 ^{c}

For opacity (%) and colour parameters (*L** for lightness, *a** for red–green, *b** for yellow–blue, and Δ*E* for total colour variation), different lowercase letters within the same column indicate significantly different values ($p < 0.05$), as determined by Tukey's HSD test.

The *a** parameter (red to green) showed no significant differences among all samples. The negative values close to zero (−0.38 to −0.80) indicate a slightly greenish colouration, almost unperceivable to the human eye. For the *b** parameter (yellow to blue), there was a significant difference between SC and ES films, which, similar to opacity and the *L** parameter, correlates with the morphological structure and molecular organisation of the films resulting from the production technique. However, no significant differences were observed between samples made using the same technique, indicating that increasing CNF content did not influence this parameter. The negative values between −1.08 and −1.42 for electrospun samples indicate a subtle tendency towards blue colouration. In contrast, SC films showed positive values between 1.78 and 2.03, indicating a slight tendency towards yellow colouration. These results align with Stoll et al. [51], who identified similar results for PLA-based films produced with bixin and acetyl tributyl citrate for active packaging. This colouration is characteristic of transparent PLA films obtained by casting, which typically exhibit positive *b** values close to 2.5.

3.2. Evaluation of Thickness and Mechanical Properties

Food packaging is essential for ensuring the protection, preservation, and safety of food products during transportation and storage until consumption. In this context, certain properties are crucial for maintaining the structural integrity, functionality, and efficiency of food packaging. Generally, PLA is brittle with low elongation at break, which limits its application in scenarios requiring high toughness or flexibility [52–54].

Therefore, the addition of cellulose nanofibers to polymeric matrices and the evaluation of different film production techniques represent a promising approach in the pursuit of enhanced properties for PLA-based films in food packaging applications. To this end, the structural behaviour and efficiency of PLA-based films reinforced with CNF produced by solvent casting and electrospinning were assessed through specific tests measuring resistance and deformation. Table 2 presents the results of thickness measurements and mechanical tests for the parameters of tensile strength (TS), elongation at break (EB), and Young's modulus.

Table 2. Thickness, tensile strength (TS), elongation at break (EB), and Young's modulus (YM) of PLA-based films reinforced with CNF by casting and electrospinning techniques.

Film	Thickness (mm)	TS (MPa)	EB (%)	YM (MPa)
Control-SC	0.06 ± 0.01^{ab}	17.4 ± 1.66^{ab}	48.8 ± 1.43^{c}	35.6 ± 3.17^{a}
CNF05-SC	0.07 ± 0.01^{ab}	18.9 ± 0.21^{ab}	44.7 ± 1.58^{bc}	42.4 ± 1.17^{a}
CNF1-SC	0.06 ± 0.02^{a}	21.6 ± 1.98^{bc}	41.8 ± 0.28^{b}	51.7 ± 4.64^{a}
Control-ES	0.08 ± 0.01^{b}	13.9 ± 2.41^{a}	7.71 ± 0.17^{a}	180 ± 32.4^{ab}
CNF05-ES	0.11 ± 0.01^{c}	25.7 ± 2.33^{c}	6.89 ± 1.49^{a}	400 ± 133.7^{c}
CNF1-ES	0.15 ± 0.01^{d}	23.6 ± 1.86^{bc}	7.67 ± 1.62^{a}	318 ± 55.7^{d}

Different lowercase letters in the same column mean values are significantly different ($p < 0.05$), as shown by Tukey's HSD test, $p < 0.05$.

The films produced by SC exhibited thickness variations between 0.06 mm and 0.07 mm, with no significant differences among the samples. This suggests that the addition of CNF did not significantly affect the thickness of the SC films. On the other hand, the films produced by ES showed greater thickness, ranging from 0.08 mm to 0.15 mm, with significant differences between the samples. The thickness increased with the addition of CNF, which can be attributed to the higher viscosity of the polymer solution containing CNF, resulting in thicker fibres during the ES process. Furthermore, the increase in film thickness may be directly related to the greater fibre diameter generated during electrospinning. This is because the higher CNF concentration contributes to an increase in the molecular weight of the entire polymeric mixture, leading to larger electrospun fibres and a wider jet diameter during the electrospinning process [26].

PLA-based films produced by solvent casting exhibited a progressive but non-significant increase in tensile strength, rising from 17.4 MPa for the control sample to 18.9 and 21.6 MPa for samples reinforced with 0.5 and 1 wt.% CNF, respectively. In contrast, electrospun films showed a significant enhancement in tensile strength with CNF addition, with values ranging from 13.9 MPa for the control to 25.7 MPa for CNF05-ES and 23.6 MPa for CNF01-ES samples. This increase indicates that CNF effectively acted as a reinforcing agent through good interaction with the nanofibril within the polymeric matrix. Furthermore, the results suggest that 0.5% CNF concentration was optimal for improving tensile properties, as demonstrated by the enhanced mechanical performance observed in both fabrication methods, confirming that PLA films became stronger and more resistant to stress at this CNF concentration, which can result from the strong interaction by hydrogen bonds between the nanofillers and matrix [55–57]. The enhancement in the tensile strength of reinforced PLA matrices has been reported by several authors [57–62]. Mazaheri et al. [59] reported a significant increase in the tensile strength of PLA/PHA films from 17.5 to 18.9 MPa with 0.3 wt.% of TEMPO-oxidised CNF, which may result in the effective interaction between nanocellulose and PLA, resulting in better chain entanglement and consequently enhanced mechanical characteristics [63]. Meng et al. [55] developed polymeric materials from renewable biomaterials based on neat PLA with a tensile strength of 63.9 MPa, which improved to 65.9 MPa with the addition of 10 wt.% CNF to the blend (PLA + CNF). Similar findings were also reported by Jonoobi et al. [62], who observed a gradual increase in tensile strength for mixtures of CNF/PLA prepared by twin screw extrusion with 1, 3, and 5 wt.% CNF, noting an increase of up to 22.4% in tensile strength with the addition of 5 wt.% CNF.

A notable difference was observed in the elongation at break (EB) between the two film production techniques. Films produced by solvent casting exhibited higher EB values (41.8–48.8%), indicating high ductility, while electrospun films showed significantly lower EB values (6.89–7.71%) and greater brittleness. This marked contrast is attributed to microstructural differences, where solvent casting produces dense, continuous films with

greater chain mobility and reorganisation capacity during deformation. In contrast, the electrospun films prepared using a flat collector (rather than a rotating drum) result in a highly entangled, randomly oriented network of fibres. This extensive physical cross-linking among fibres severely constrains molecular mobility and prevents the film from stretching, leading to the observed brittle, plastic behaviour instead of elastic deformation. Further, local crystalline domains within individual fibres can increase rigidity, but the dominant factor is the extensive fibre entanglement and limited chain mobility inherent to the random fibrous mat [58,64], as detailed in Section 3.5.

When examining the samples produced by electrospinning and comparing the influence of CNF, the elongation at break remained relatively unchanged. This demonstrates that in this case, the elasticity of the films was not significantly affected by the introduction of the nanofibers. On the other hand, for samples produced by solvent casting, increasing the nanofibres concentration significantly reduced elasticity by 2 wt.% CNF (48.8%) compared to the control sample (41.8%). Trivedi & Gupta [33] observed similar behaviour in PLA-based filaments with crystalline nanocellulose (CNC) and PLA, where the PLA and CNC 1 wt.% mixture showed an elongation at break of 46.1%, which decreased to 27.8% and 16.1% for mixtures with 3 and 5 wt.% CNC, respectively. This more brittle behaviour may be associated with the ability of nanofillers to reduce the ductility of polymeric materials, making them more rigid and less elastic depending on the incorporated concentration.

Young's modulus is a crucial parameter for evaluating films, as it indicates material stiffness, with an observed improvement in films produced with CNF by both techniques. Films produced by SC showed YM of 35.6 MPa (control), which increased to 42.4 and 51.7 MPa with 0.5 and 1 wt.% CNF incorporation, respectively. However, this increase was not statistically significant. Conversely, ES-produced films exhibited a significant increase with CNF incorporation. The control sample showed a YM of 180 MPa, whilst samples reinforced with 0.5 and 1% displayed YM of 400 and 318 MPa, respectively. When CNF is added, the film rigidity increases due to its crystalline structure. Similar results have been reported in previous studies [57,61,62,64,65]. The notably higher YM in ES films stems from molecular orientation during fibre formation, and enhanced crystallinity is due to strain-induced crystallisation during electrospinning [66,67].

Overall, these findings demonstrated that CNF functions as an excellent reinforcing agent in PLA films, enhancing their mechanical properties and showing the potential of these samples for use in the food packaging industry.

3.3. Physical Characterisation

Table 3 summarises the water resistance properties of PLA-based films (control) and films reinforced with CNF produced via SC and ES methods. Overall, SC films exhibit higher moisture content compared to ES films. However, SC films maintain stable moisture levels regardless of CNF content, with values ranging from 7.49% for Control-SC, 8.15% for CNF05-SC, and 7.95% for CNF1-SC, showing no significant differences between the samples.

On the other hand, the addition of CNF significantly increases the moisture content in ES films, particularly for the sample containing 0.5% CNF (CNF05-ES) compared to the control sample (Control-ES). This suggests that the hydrophilic nature of nanofibres contributes to increased moisture absorption. Nanofibres typically possess a large surface area and numerous exposed hydroxyl groups that interact with water molecules, enhancing moisture absorption capacity [68,69]. Furthermore, in electrospun films, the fibrous and porous structure facilitates water retention by creating additional pathways for diffusion and adsorption of water molecules within the film matrix [69].

Table 3. Moisture content, solubility, and water vapor permeability (WVP) of PLA-based films reinforced with CNF by casting and electrospinning techniques.

Film	Moisture (%)	Solubility (%)	WVP *
Control-SC	7.49 ± 0.65 ^{c}	0.90 ± 0.38 ^{a}	0.07 ± 0.01 ^{a}
CNF05-SC	8.15 ± 0.79 ^{c}	0.90 ± 0.88 ^{a}	0.08 ± 0.01 ^{a}
CNF1-SC	7.95 ± 0.77 ^{c}	0.45 ± 0.19 ^{a}	0.06 ± 0.01 ^{a}
Control-ES	3.51 ± 0.95 ^{a}	2.16 ± 0.46 ^{a}	1.28 ± 0.01 ^{b}
CNF05-ES	6.42 ± 0.99 ^{bc}	1.90 ± 0.51 ^{a}	1.77 ± 0.01 ^{c}
CNF1-ES	4.62 ± 0.93 ^{ab}	1.81 ± 0.58 ^{a}	2.39 ± 0.02 ^{d}

Values with different lowercase letters in the same column are significantly different ($p < 0.05$), as determined by Tukey's HSD test.; * WVP: Water Vapor Permeability (* 10^{-10} g·m^{-2}·s^{-1} Pa^{-1}).

In this context, the stability in moisture content observed in SC-produced films can be attributed to their denser and more homogeneous structure, formed during the slow solvent evaporation process. The continuous and compact polymer matrix hinders the access of water molecules to hydrophilic sites on CNF, reducing overall absorption capacity [68]. Additionally, nanofibres may be better dispersed within SC-produced films, minimising the formation of aggregates that could retain more water.

The high moisture content observed in ES-reinforced films is closely linked to the increased number of hydrophilic sites able to form hydrogen bonds with water molecules. The open and porous structure of these films promotes the exposure of hydroxyl (-OH) groups present in the cellulose nanofibrils, thereby enhancing the affinity for water and facilitating both moisture uptake and retention [70,71]. By contrast, films produced by solvent casting (SC) form denser and more homogeneous polymer matrices, in which hydrophilic sites are partially concealed or less accessible, thereby limiting the formation of hydrogen bonds between water and the polymer. Consequently, SC films exhibit greater stability in humid environments and provide improved performance as moisture barriers, essential qualities for applications such as food packaging, where preventing water migration is critical.

The solubility of PLA-based control films and films reinforced with 0.5% or 1% CNF loading, produced by solvent casting (SC) and electrospinning (ES), was determined by immersion in water for 7 days. ES-produced films present higher water solubility (1.81–2.16%) than SC films (<1%), irrespective of CNF loading. Although increasing CNF to 1% slightly reduces solubility in both SC and ES films, the differences are not statistically significant (Table 3). This reduced solubility may result from enhanced intermolecular interactions caused by the presence of CNF in the polymeric matrix [72,73]. Higher nanofibres content promotes cross-linking within the film matrix, increasing structural cohesion and hindering water penetration [74,75]. These effects collectively reduce water absorption and dissolution susceptibility in the polymeric matrix.

The WVP results presented in Table 3 show no significant differences among films manufactured using the solvent casting (SC) technique, with all presenting (Control-SC, CNF05-SC, and CNF1-SC) lower WVP values (ranging from 0.06–0.08 × 10^{-10} g·m^{-2}·s^{-1}·Pa^{-1}) when compared to their electrospun counterparts, indicating superior barrier performance.

On the other hand, electrospun films showed significantly higher WVP values overall, with Control-ES exhibiting approximately 18 times greater permeability (1.28 × 10^{-10} g·m^{-2}·s^{-1}·Pa^{-1}) than its SC counterpart. Furthermore, the addition of CNF to electrospun films significantly increased the WVP in a concentration-dependent way. CNF05-ES showed a 38% increase in WVP compared to Control-ES, while CNF1-ES exhibited an 87% increase. These contrasting trends between manufacturing methods suggest that the structural organisation of polymer chains and nanofibres fundamentally differs between SC and ES

techniques. This observation aligns with Saeb et al. [76], who stated that WVP is influenced by the internal structure of each film. The incorporation of CNF appears to interfere with the continuity of the PLA matrix in ES films, making the structure more susceptible to water vapour diffusion. This effect becomes more pronounced with increasing CNF concentration, suggesting potential aggregation or weak interfacial adhesion at higher loads. The counterintuitive impact of CNF on ES films, where various nanomaterials typically enhance barrier properties by creating complex and morphologically distinct structures [77–79], warrants further investigation into fibre morphology, CNF dispersion quality, and potential hygroscopic effects that may compromise the intended barrier improvements.

3.4. Evaluation of Water Contact Angle (WCA)

Figure 4 presents the water contact angle (WCA) measurements of films produced by electrospinning (ES) and solvent casting (SC), both reinforced with cellulose nanofibres (CNF), alongside their respective control samples. The WCA values serve as indicators of the hydrophobicity of these materials. Values below 90° signify hydrophilic behaviour, while values equal to or greater than 90° denote hydrophobic characteristics.

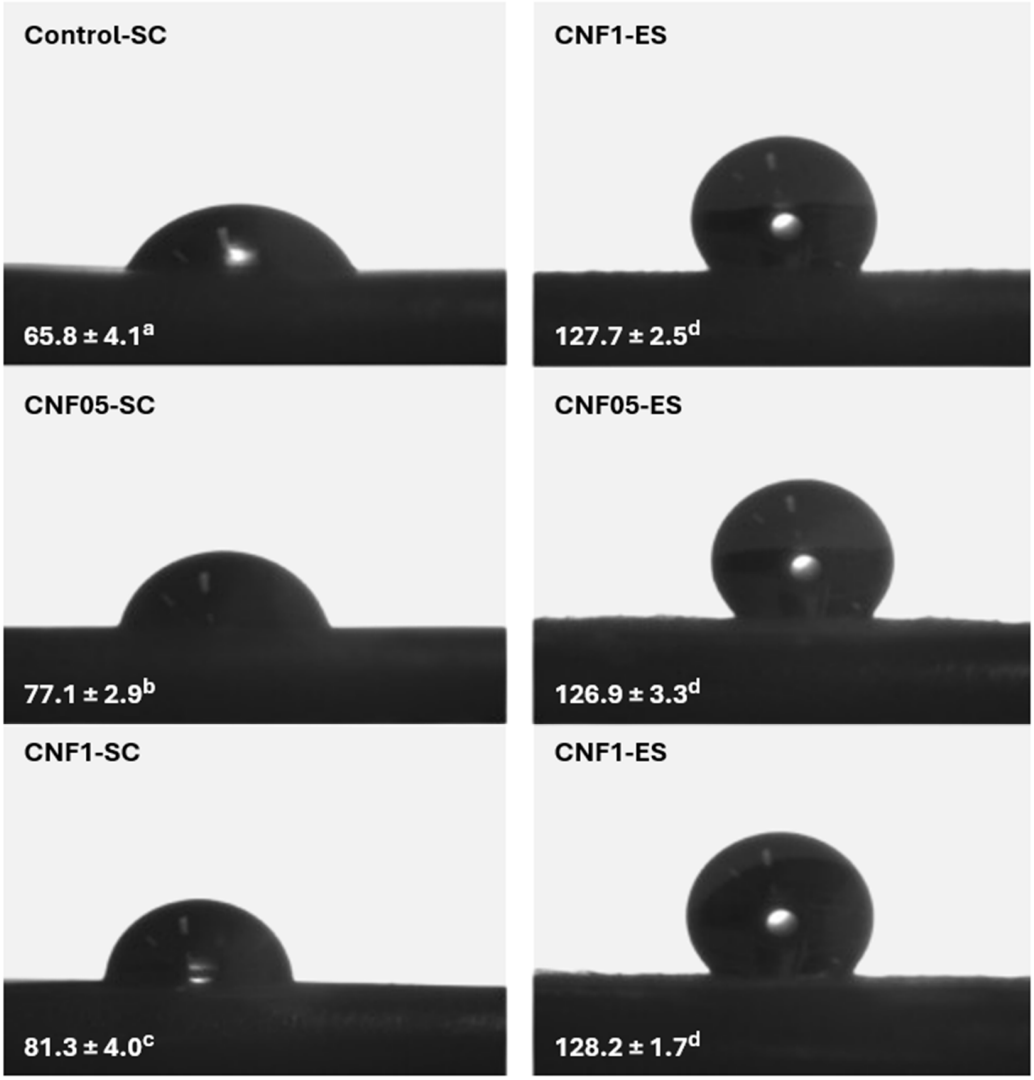

Figure 4. Water Contact Angle of PLA-based films reinforced with CNF by solvent casting (SC) and electrospinning (ES) with respective controls (without CNF). Different lowercase letters indicate significant differences between the samples ($p < 0.05$).

All the films produced via ES exhibited a pronounced degree of surface hydrophobicity, with WCA values ranging from 126.9° to 128.2°. Typically, materials displaying such hydrophobic character are expected to demonstrate low water vapour permeability. However, this was not observed in the ES films. Although the remarkable hydrophobicity measured at the surface would generally be associated with superior water vapour barrier properties, the ES films displayed significantly higher water vapour permeability (WVP) compared to those produced by the solvent casting technique.

This seemingly paradoxical result suggests that elevated surface hydrophobicity alone did not suffice to impede water vapour transmission in the ES films. The likely explanation lies in their internal microstructure. While electrospinning generates externally smooth and homogeneous surfaces, attributable to the use of a fixed stainless-steel collector during nanofibre deposition, the resultant internal architecture is relatively loose and porous. This facilitates water vapour transport through the network, explaining the much higher permeability despite the highly hydrophobic surface.

Argel-Pérez et al. [80] reported that enhancing the hydrophobicity of coatings composed of PLA and cocoa butter, stabilised with cellulose nanofibres, led to improved water vapour barrier performance due to the smooth, well-organised surface structure of the resulting films. In the present study, however, the less organised internal fibre arrangement in the ES films appears to override the influence of surface characteristics, limiting barrier efficacy despite high WCA values.

In contrast, the SC films displayed moderately hydrophilic behaviour, with WCA readings between 65.8° and 81.3°. This outcome may be attributed to their higher density and the greater prevalence of crystalline regions, which restrict water vapour passage even in the absence of pronounced surface hydrophobicity. It is also noteworthy that increasing the CNF content within the SC films led to a reduction in hydrophilicity, evidenced by higher WCA values. This indicates that CNF addition contributes effectively to enhanced barrier properties, acting to reinforce and restructure the polymer matrix.

Deng et al. [81] proposed that the hydrophobicity of surfaces produced by electrospinning and solvent casting is governed by distinct mechanisms. In this sense, these findings underscore the necessity of considering both surface features and internal microstructure when developing films with optimised barrier performance. Surface hydrophobicity alone does not ensure low water vapour permeability. Internal organisation, density and the presence of cellulose nanofibres all play crucial roles in determining the overall effectiveness of the barrier material.

The paradoxical observation of high surface hydrophobicity coupled with elevated water vapour permeability in ES films represents a significant finding, demonstrating that the internal microstructure dominates the barrier performance, regardless of the surface properties. This insight is critical for rational material design, as it indicates that enhancing surface hydrophobicity alone cannot ensure barrier functionality in porous fibrous structures.

3.5. Morphological Characterisation

Figure 5 shows the micrographs of PLA-based films (control and those reinforced with 0.5% and 1% CNF). The morphology of the isolated CNF used as reinforcement, characterised by TEM and SEM, was reported in our previous work [6]. The SEM images show that the microstructures of films produced by solvent casting (SC) and electrospinning (ES) are distinctly different. Whilst films produced by SC exhibit a predominantly smooth and flat morphology with few structural elements visible on the surface, the ES films display three-dimensional fibrous structures forming interconnected networks with greater porosity and surface area.

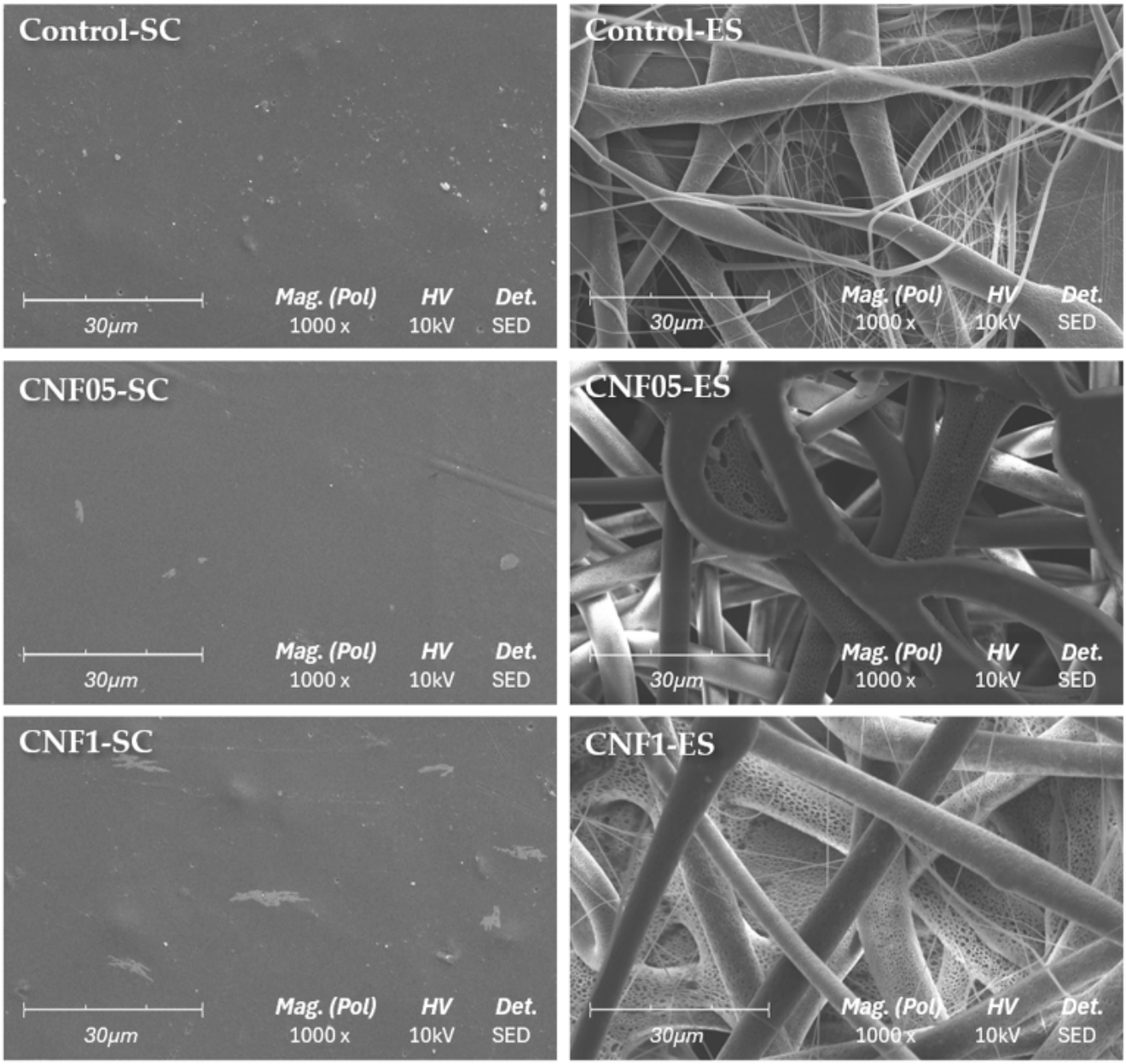

Figure 5. SEM micrographs (30 µm; 1000×) of PLA-based films reinforced with CNF by solvent casting (SC) and electrospinning (ES) with respective controls (without CNF).

In the present work, the comparison between films obtained by SC and ES was primarily intended to discuss how differences in microstructural morphology (continuous and dense films in the case of SC versus a highly porous fibrous network in the case of ES) are reflected in the final properties of the materials, rather than to establish a hierarchy of efficiency between the fabrication processes.

The microstructure of the Control-SC film presented a completely uniform and smooth surface, virtually without texture or significant microstructural elements. The incorporation of 0.5% CNF showed a homogeneous dispersion of CNF in the polymer matrix. While the film morphology became more pronounced with the incorporation of 1% CNF, which, despite maintaining the predominantly smooth morphology observed before, exhibited more evident surface roughness due to the increased concentration of CNF. Similarly, Costa et al. [82] reported that increasing nanocellulose concentration resulted in more irregular and rough morphological structures in chitosan-based films.

The films produced by ES showed a structure composed of a network of randomly distributed fibres. No micron-sized CNF agglomerates were detected on the fibre surfaces in any condition, suggesting that CNF remained efficiently dispersed at the nanoscale within the PLA matrix. The Control-ES sample displayed irregular fibres where smaller-diameter fibres were interspersed among thicker ones, forming a mesh with inter-fibre pores. The addition of 0.5% CNF (CNF05-ES) resulted in fibres with larger diameters, whilst still maintaining the irregular pattern of the control-ES sample. Conversely, the 1% CNF incorporated (CNF1-ES) sample micrograph seems to exhibit a more regular fibrous network with morphological characteristics distinct from the control film fibres. Thus, the ES films seem to demonstrate more clearly the influence of CNF on the final material structure, where the addition of 0.5% and 1% resulted in films with distinct morphologies, particularly notable when compared to the neat PLA-based films. This result corroborates other studies demonstrating that the addition of various nanofibres/nanoparticles to electrospun PLA matrices significantly affects material morphology [11,65,83,84].

3.6. Thermal Stability

Thermogravimetric analysis (TGA) was conducted to evaluate the thermal stability of the samples. The thermogravimetric (TG) and derivative thermogravimetric (DTG) curves for both the control and CNF-reinforced films, produced via solvent casting (SC) and electrospinning (ES), are presented in Figure 6A,B.

The TG curves (Figure 6A) reveal that all films, regardless of the production method or CNF concentration, exhibited a similar three-stage degradation pattern. The first stage, occurring between 50 °C and 120 °C, corresponds to the evaporation of water molecules, with weight losses ranging from 3% to 7%. This stage was more pronounced in SC films above 90 °C, with a peak at 151 °C for the control sample (Control-SC). For each film, T_{max} (10%) and the weight of remaining ash (%) for the second stage of thermal decomposition are summarised in Supplementary Table S2.

The absence of additional temperature-lowering and mass loss events in any of the samples indicates that no detectable residual chloroform remained in the dried films, supporting the efficiency of the solvent removal protocol used prior to characterisation.

The second stage of thermal degradation occurred similarly across all films, regardless of production method. The most significant weight loss was observed between 290 °C and 330 °C. The thermal degradation trends for PLA-based films were comparable to those observed in pure PLA, indicating relative stability. However, SC films reinforced with CNF (CNF05-SC and CNF1-SC) exhibited lower onset degradation temperatures, suggesting slightly reduced thermal stability. This observation aligns with the findings of Zhang et al. [83], who reported similar behaviour in PLA composite films containing nanocellulose. Additionally, all ES films showed lower initial degradation temperatures compared to SC films. This behaviour may be explained by the limited amorphous zones in electrospun films, which reduce their thermal stability. In the third stage, thermal degradation began around 320 °C but occurred less sharply compared to earlier stages.

Overall, SC films demonstrated slightly higher thermal stability compared to their ES counterparts. The maximum degradation temperature (T_{max}) for Control-SC was approximately 328 °C, while Control-ES exhibited a lower T_{max} of around 314 °C. This difference can be attributed to structural variations arising from the processing methods. Solvent casting involves slow solvent evaporation, which promotes the formation of more organised and oriented crystalline domains [29]. In contrast, electrospinning subjects the polymer solution to rapid stretching and instantaneous solvent evaporation, resulting in less organised molecular arrangements with limited time for their alignment in crystalline regions formation [29,84].

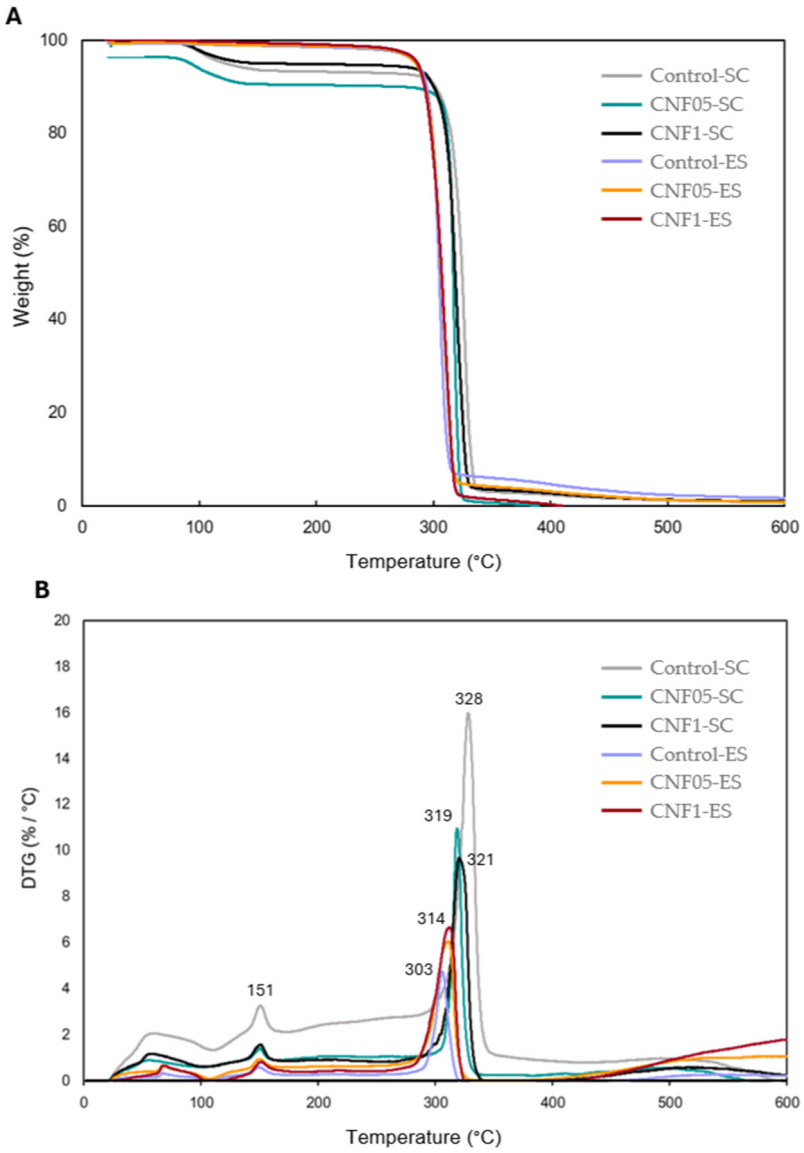

Figure 6. (**A**) Thermogravimetric analysis (TGA) and (**B**) DTG curves of PLA-based films with CNF by solvent casting (SC) and electrospinning (ES).

The incorporation of CNF influenced the thermal stability of both SC and ES films. For SC films, adding 0.5% CNF (CNF05-SC) reduced T_{max} to 319 °C compared to the control (328 °C), while 1% CNF (CNF1-SC) slightly increased T_{max} to 321 °C. For ES films, thermal degradation peaks were consistently lower than those of their SC counterparts, with CNF-reinforced samples showing peaks around 303 °C.

3.7. ATR-FTIR: Chemical and Structural Characterization

In a previous study by our group, the CNFs isolated from *S. ramosissima* were fully characterised by TEM and FTIR, displaying the typical cellulose absorption bands and nanoscale fibrillar morphology expected for enzymatically produced CNF [6]. Figure 7 presents the ATR-FTIR spectra of PLA films, both with and without CNF reinforcement. The spectra reveal characteristic PLA bands in all analysed samples, confirming the fundamental chemical structure of the polymer. The main observed bands include C-H stretching in the 2985 cm^{-1} region, the intense C=O stretching band at approximately 1747 cm^{-1} characteristic of the PLA ester group, CH_3 angular deformations at 1456 cm^{-1} and 1358 cm^{-1}, C-O-C stretching in the 1180–1080 cm^{-1} region, and C-C vibration around 756 cm^{-1} [85–87].

These bands were identified in all spectra, regardless of the film production method or CNF concentration used, suggesting that PLA's primary chemical structure remains preserved even after reinforcement incorporation at the studied concentrations (0.5–1 wt.%). Although CNF represents only 0.5–1 wt.% of the formulation and its characteristic bands overlap with intense PLA absorptions, a weak shoulder near 1254 cm^{-1}, assigned to C–O stretching of cellulose, can still be distinguished in CNF-reinforced films, supporting the presence of CNF within the PLA matrix.

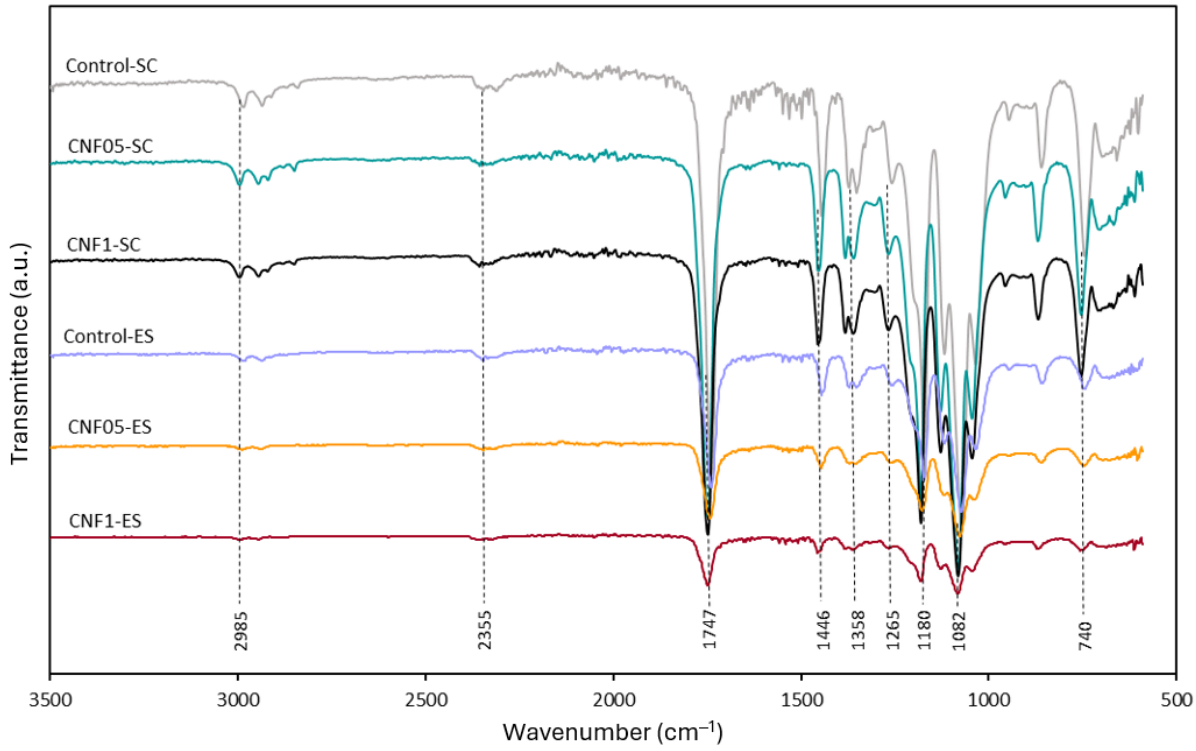

Figure 7. Attenuated total reflectance–Fourier transform infrared (ATR-FTIR) spectra of PLA-based films reinforced with CNF). ATR-FTIR spectra, for each film, are shown as absorbance values (in arbitrary units (A.U.).

Comparison between spectra reveals significant differences between films produced by solvent casting (SC) and electrospinning (ES). The SC film spectra exhibit higher absorption intensity compared to their ES counterparts, particularly in the characteristic PLA regions. This difference can be attributed to the distinct morphology obtained through different processing methods, as electrospinning produces fibrillar structures with diameters typically ranging from 160–190 nm, resulting in lower density and more random molecular orientation [63,64]. In the C-O-C stretching region (1200–1000 cm^{-1}), electrospun films show slight alterations in relative band intensity, possibly induced by the rapid stretching and solvent evaporation during fibre formation [27,88].

In films with CNF addition, especially at 1% concentration, an increase in band intensity was observed in the 3000–2940 cm^{-1} region, corresponding to C-H stretching. Also notable is the presence of a peak at approximately 1254 cm^{-1}, which confirms the C-O stretching vibrations of CNF present in the polymeric matrix [6]. This region shows more pronounced alterations in samples with higher CNF concentration (1%), indicating that the interaction between CNF and the polymeric matrix intensifies with increasing reinforcement concentration [74,89].

The modifications observed in the FTIR spectra correlate directly with the mechanical and thermal properties of the nanocomposites. Huan et al. [90] and Keeratipinit et al. [74]

demonstrated in previous studies that adding CNF at concentrations of 1% can significantly increase the tensile modulus and tensile strength in PLA/CNF composites. This behaviour can be explained by the good dispersion of nanocellulose in the PLA matrix, where CNF act as a nucleating agent, promoting higher crystallinity and improving stress transfer at the reinforcement–matrix interface, as evidenced by the alterations in characteristic bands in the FTIR spectra [89]. Furthermore, CNF contributes to improved thermal stability, as evidenced in this study and previous research reporting increases in decomposition temperature [91,92]. The slight shifts observed in the carbonyl group bands in reinforced films suggest the occurrence of intermolecular interactions between PLA and CNF, possibly through hydrogen bonding between the hydroxyl groups of cellulose and the carbonyl groups of PLA resulting in a more rigid and thermally stable matrix [89].

3.8. Assessment of the Performance of Packaging in HPP

Figure 8 presents the proof of concept for PLA-based films produced via the solvent casting (SC) technique. Visual inspection before and after processing reveals the potential of "pouch"-type packaging fabricated from PLA-based films reinforced with varying concentrations of CNF for high-pressure processing (HPP) applications.

Figure 8. "Pouch-type" food packaging made from PLA-based films reinforced with CNF by solvent casting (SC) during the proof of concept in HPP.

The packaging maintained overall structural integrity after exposure to 500 MPa for 5 min at 25 °C (typical conditions for HPP commercial pasteurisation), conditions that pose

significant challenges for most polymeric materials. This behaviour is particularly notable for biodegradable materials such as PLA, which typically exhibit inferior mechanical properties compared to conventional plastics. Hydrostatic pressure in HPP systems is uniformly transmitted through packaging materials [93–95]. However, inadequate materials may experience deformation or structural failure under HPP conditions [96].

The absence of significant ruptures or leaks post-processing suggests that the tested packaging holds promise for HPP applications. This finding is significant given that biodegradable materials often face limitations in mechanical and barrier properties compared to conventional counterparts [97]. In this sense, the importance of developing HPP-compatible packaging materials is a critical factor for expanding this preservation technology. CNF-reinforced PLA represents a promising approach to simultaneously address sustainability demands and HPP compatibility. Furthermore, as shown in this study and others, incorporating CNF into PLA matrices can markedly enhance mechanical strength, barrier properties, and permeability [98,99].

Finally, the use of *S. ramosissima* as a test product is strategic, as it is a solid food subjected to hydrostatic pressure and is increasingly recognised as a functional food [100,101]. Additionally, this work sets a precedent for future studies on *S. ramosissima* shelf-life improvement, a highly perishable and seasonal product.

4. Conclusions

The present study successfully developed and characterised PLA-based biocomposite films reinforced with cellulose nanofibres (CNFs) derived from the by-product of *S. ramosissima*, employing both solvent casting (SC) and electrospinning (ES) techniques. SC films exhibited a homogeneous and transparent morphology, with superior moisture barrier performance and greater ductility, while ES films presented fibrous and porous structures, resulting in higher tensile strength and rigidity but leading to increased fragility and moisture permeability. Notably, ES films showed higher contact angles, reflecting greater hydrophobicity, despite lower efficiency as a water vapour barrier. This outcome demonstrates that, whilst hydrophobicity is commonly perceived as a key factor for enhancing vapour barrier performance, the actual effectiveness is governed by a complex interplay of structural and chemical attributes specific to each polymer matrix. In the present study, the dominance of internal organisation, density and the distribution of nanofibres was evident, as the less hydrophobic SC films surpassed the ES films in water vapour barrier capability. The comprehensive characterisation revealed non-intuitive structure–property relationships, particularly the decoupling of surface hydrophobicity from barrier performance in electrospun films, providing quantitative guidelines for the rational optimisation of material design. Incorporation of CNF (0.5–1 wt.%) significantly improved mechanical performance, particularly tensile strength and Young's modulus, with 0.5% CNF identified as the optimal reinforcement concentration. Thermal and spectroscopic analyses confirmed effective integration of CNF into the PLA matrix without compromising thermal stability. Notably, pouch-type packages produced from SC films, both with and without CNF, withstood high-pressure processing (HPP) conditions (500 MPa, 5 min, 25 °C) without rupture or leakage, demonstrating their technical feasibility for industrial food packaging applications. SC films were selected for HPP validation based on their superior barrier and mechanical properties for flexible packaging applications, withstanding industrial HPP conditions. These findings establish technical feasibility pathways for industrial implementation of CNF-reinforced biopolymer packaging compatible with HPP technology, contributing to circular economy strategies and sustainable packaging development.

Supplementary Materials: The following supporting information can be downloaded at https://www.mdpi.com/article/10.3390/app152413247/s1, Table S1: Experimental design for the preparation of PLA-based films by solvent casting (SC) and electrospinning (ES), showing the combination of processing technique, formulation and PLA/CNF concentrations used in each experimental condition; Table S2: TGA values at the second stage of thermal decomposition of PLA-based films (control) and reinforced with CNF.

Author Contributions: Conceptualisation, A.R.L. and M.C.V.; Methodology, A.R.L., N.L.C., J.A.S. and M.C.V.; Investigation, A.R.L., N.L.C., I.D., R.A.A. and M.C.V.; Writing—original draft preparation, A.R.L. and N.L.C.; Writing—review and editing, A.R.L., N.L.C., J.A.S. and M.C.V.; Supervision, M.C.V. and J.A.S.; and Funding acquisition, A.R.L., J.A.S. and M.C.V. All authors have read and agreed to the published version of the manuscript.

Funding: The authors further acknowledge the R&D unit MED—Mediterranean Institute for Agriculture, Environment and Development (https://doi.org/10.54499/UIDB/05183/2020; https://doi.org/10.54499/UIDP/05183/2020) (accessed on 7 December 2025) and the Associate Laboratory CHANGE—Global Change and Sustainability Institute (https://doi.org/10.54499/LA/P/0121/2020) (accessed on 7 December 2025) and project UIDB/50006/2020 and UIDP/50006/2020—Laboratório Associado para a Química Verde—66 e Processos Limpos. The scholarships of the first second and fourth authors, A.R.L., N.L.C. and R.A.A., were funded by the Portuguese Foundation for Science and Technology (FCT) through FCT PhD grants https://doi.org/10.54499/SFRH/BD/149398/2019; https://doi.org/10.54499/SFRH/BD/149395/2019 (accessed on 7 December 2025) and SFRH/BD/146009/2019, respectively.

Institutional Review Board Statement: Not applicable.

Informed Consent Statement: Not applicable.

Data Availability Statement: The original contributions presented in the study are included in the article. Further inquiries can be directed to the corresponding author.

Acknowledgments: The authors acknowledge Miguel Salazar and Carla Nunes from RiaFresh® (Faro, Portugal) for their support in this project, kindly providing the *Salicornia ramosissima* agro-industrial by-products.

Conflicts of Interest: The authors declare no conflicts of interest.

References

1. European Parliament. *Regulation (EU) 2025/40 of the European Parliament and the Council of 19 December 2024 on Packaging and Packaging Waste, Amending Regulation (EU) 2019/1020 and Directive (EU) 2019/904, and Repealing Directive 94/62/EC*; Publications Office of the European Union: Brussels, Belgium, 2025; Volume 40.
2. United Nations Transforming Our World: The 2030 Agenda for Sustainable Development. Available online: https://sustainabledevelopment.un.org/post2015/transformingourworld (accessed on 7 December 2025).
3. Vinitskaia, N.; Lindstad, A.J.; Lev, R.; Kvikant, M.; Xu, C.; Leminen, V.; Li, K.D.; Pettersen, M.K.; Grönman, K. Environmental Sustainability, Food Quality and Convertibility of Bio-Based Barrier Coatings for Fibre-Based Food Packaging: A Semisystematic Review. *Packg. Techn. and Sci.* **2024**, *38*, 255–280. [CrossRef]
4. Cristofoli, N.L.; Lima, A.R.; Tchonkouang, R.D.N.; Quintino, A.C.; Vieira, M.C. Advances in the Food Packaging Production from Agri-Food Waste and By-Products: Market Trends for a Sustainable Development. *Sustainability* **2023**, *15*, 6153. [CrossRef]
5. Coelho, C.C.S.; Michelin, M.; Cerqueira, M.A.; Gonçalves, C.; Tonon, R.V.; Pastrana, L.M.; Freitas-Silva, O.; Vicente, A.A.; Cabral, L.M.C.; Teixeira, J.A. Cellulose Nanocrystals from Grape Pomace: Production, Properties and Cytotoxicity Assessment. *Carbohydr. Polym.* **2018**, *192*, 327–336. [CrossRef] [PubMed]
6. Lima, A.R.; Cristofoli, N.L.; Rosa da Costa, A.M.; Saraiva, J.A.; Vieira, M.C. Comparative Study of the Production of Cellulose Nanofibers from Agro-Industrial Waste Streams of Salicornia Ramosissima by Acid and Enzymatic Treatment. *Food and Bioprod. Process.* **2023**, *137*, 214–225. [CrossRef]
7. Tibolla, H.; Pelissari, F.M.; Martins, J.T.; Vicente, A.A.; Menegalli, F.C. Cellulose Nanofibers Produced from Banana Peel by Chemical and Mechanical Treatments: Characterization and Cytotoxicity Assessment. *Food Hydrocoll.* **2018**, *75*, 192–201. [CrossRef]
8. Ventura-Cruz, S.; Tecante, A. Extraction and Characterization of Cellulose Nanofibers from Rose Stems (*Rosa* Spp.). *Carbohydr. Polym.* **2019**, *220*, 53–59. [CrossRef]

9. Talebi, H.; Ghasemi, F.A.; Ashori, A. The Effect of Nanocellulose on Mechanical and Physical Properties of Chitosan-Based Biocomposites. *J. Elast. Plast.* **2022**, *54*, 22–41. [CrossRef]
10. Zhao, L.; Duan, G.; Zhang, G.; Yang, H.; Jiang, S.; He, S. Electrospun Functional Materials toward Food Packaging Applications: A Review. *Nanomaterials* **2020**, *10*, 150. [CrossRef]
11. Bamian, M.; Pajohi-Alamoti, M.; Azizian, S.; Nourian, A.; Tahzibi, H. An Electrospun Polylactic Acid Film Containing Silver Nanoparticles and Encapsulated Thymus Daenensis Essential Oil: Release Behavior, Physico-Mechanical and Antibacterial Studies. *J. Food Meas. Charact.* **2023**, *17*, 3450–3463. [CrossRef]
12. Stark, N.M. Opportunities for Cellulose Nanomaterials in Packaging Films: A Review and Future Trends. *J. Renew Mater.* **2016**, *4*, 313–326. [CrossRef]
13. Blanco, A.; Monte, M.C.; Campano, C.; Balea, A.; Merayo, N.; Negro, C. *Nanocellulose for Industrial Use: Cellulose Nanofibers (CNF), Cellulose Nanocrystals (CNC), and Bacterial Cellulose (BC)*; Elsevier Inc.: Amsterdam, The Netherlands, 2018; ISBN 9780128133514.
14. Trivedi, A.K.; Gupta, M.K.; Singh, H. PLA Based Biocomposites for Sustainable Products: A Review. *Advan. Indust, and Eng. Polym. Resear.* **2023**, *6*, 382–395. [CrossRef]
15. Rezvani Ghomi, E.; Khosravi, F.; Saedi Ardahaei, A.; Dai, Y.; Neisiany, R.E.; Foroughi, F.; Wu, M.; Das, O.; Ramakrishna, S. The Life Cycle Assessment for Polylactic Acid (PLA) to Make It a Low-Carbon Material. *Polymers* **2021**, *13*, 1854. [CrossRef] [PubMed]
16. Islam, M.M.; Chaudry, S.; Thornton, A.W.; Haque, N.; Lau, D.; Bhuiyan, M.; Pramanik, B.K. Environmental Footprint of Polylactic Acid Production Utilizing Cane-Sugar and Microalgal Biomass: An LCA Case Study. *J. Clean. Prod.* **2025**, *496*, 145132. [CrossRef]
17. Hussain, M.; Khan, S.M.; Shafiq, M.; Abbas, N. A Review on PLA-Based Biodegradable Materials for Biomedical Applications. *Giant.* **2024**, *18*, 100261. [CrossRef]
18. Grand View Research Polylactic Acid Market Size & Trends. Available online: https://www.grandviewresearch.com/industry-analysis/polylactic-acid-pla-market (accessed on 29 April 2025).
19. Ruz-Cruz, M.A.; Herrera-Franco, P.J.; Flores-Johnson, E.A.; Moreno-Chulim, M.V.; Galera-Manzano, L.M.; Valadez-González, A. Thermal and Mechanical Properties of PLA-Based Multiscale Cellulosic Biocomposites. *J. Mater. Resear. Tech.* **2022**, *18*, 485–495. [CrossRef]
20. Ren, Q.; Wu, M.; Wang, L.; Zheng, W.; Hikima, Y.; Semba, T.; Ohshima, M. Cellulose Nanofiber Reinforced Poly (Lactic Acid) with Enhanced Rheology, Crystallization and Foaming Ability. *Carbohydr. Polym.* **2022**, *286*, 191320. [CrossRef]
21. Plamadiala, I.; Croitoru, C.; Pop, M.A.; Roata, I.C. Enhancing Polylactic Acid (PLA) Performance: A Review of Additives in Fused Deposition Modelling (FDM) Filaments. *Polymers* **2025**, *17*, 191. [CrossRef]
22. Xue, J.; Wu, T.; Dai, Y.; Xia, Y. Electrospinning and Electrospun Nanofibers: Methods, Materials, and Applications. *Chem. Rev.* **2019**, *119*, 5298–5415. [CrossRef]
23. Thabet, Y.; Breitkreutz, J. Orodispersible Films: Product Transfer from Lab-Scale to Continuous Manufacturing. *Int. J. Pharm.* **2018**, *535*, 285–292. [CrossRef]
24. Kong, I.; Tshai, K.Y.; Enamul Hoque, M. Manufacturing of Natural Fibre-Reinforced Polymer Composites by Solvent Casting Method. In *Manufacturing of Natural Fibre Reinforced Polymer Composites*; Salit, M., Jawaid, M., Yusoff, N., Hoque, M., Eds.; Springer: Cham, Switzerland; pp. 331–349. ISBN 978-3-319-07944-8.
25. Senthil Muthu Kumar, T.; Senthil Kumar, K.; Rajini, N.; Siengchin, S.; Ayrilmis, N.; Varada Rajulu, A. A Comprehensive Review of Electrospun Nanofibers: Food and Packaging Perspective. *Compos. B Eng.* **2019**, *175*, 107074. [CrossRef]
26. Abdulhussain, R.; Adebisi, A.; Conway, B.R.; Asare-Addo, K. Electrospun Nanofibers: Exploring Process Parameters, Polymer Selection, and Recent Applications in Pharmaceuticals and Drug Delivery. *J. Drug Deliv. Sci. Technol.* **2023**, *90*, 105156. [CrossRef]
27. Jacobs, V.; Anandjiwala, R.D.; Maaza, M. The Influence of Electrospinning Parameters on the Structural Morphology and Diameter of Electrospun Nanofibers. *J. Appl. Polym. Sci.* **2009**, *115*, 3130–3136. [CrossRef]
28. Maduna, L.; Patnaik, A. Challenges Associated with the Production of Nanofibers. *Processes* **2024**, *12*, 2100. [CrossRef]
29. Ghosal, K.; Chandra, A.; Praveen, G.; Snigdha, S.; Roy, S.; Agatemor, C.; Thomas, S.; Provaznik, I. Electrospinning over Solvent Casting: Tuning of Mechanical Properties of Membranes. *Sci. Rep.* **2018**, *8*, 5058. [CrossRef] [PubMed]
30. Topuz, F.; Uyar, T. Electrospinning of Sustainable Polymers from Biomass for Active Food Packaging. *Sustain. Food Technol.* **2024**, *2*, 1266–1296. [CrossRef]
31. Borah, A.R.; Hazarika, P.; Duarah, R.; Goswami, R.; Hazarika, S. Biodegradable Electrospun Membranes for Sustainable Industrial Applications. *ACS Omega* **2024**, *9*, 11129–11147. [CrossRef]
32. Song, J.; Lin, X.; Ee, L.Y.; Li, S.F.Y.; Huang, M. A Review on Electrospinning as Versatile Supports for Diverse Nanofibers and Their Applications in Environmental Sensing. *Adv. Fiber Mater.* **2023**, *5*, 429–460. [CrossRef]
33. Shiri, A.; Sadeghi, E.; Abdolmaleki, K.; Dabirian, F.; Shirvani, H.; Soltani, M. Eco-Friendly and Smart Electrospun Food Packaging Films Based on Polyvinyl Alcohol and Sumac Extract: Physicochemical, Mechanical, Antibacterial, and Antioxidant Properties. *Food Sci. Nutr.* **2025**, *13*, e70190. [CrossRef]

34. Melendez-Rodriguez, B.; Castro-Mayorga, J.L.; Reis, M.A.M.; Sammon, C.; Cabedo, L.; Torres-Giner, S.; Lagaron, J.M. Preparation and Characterization of Electrospun Food Biopackaging Films of Poly(3-Hydroxybutyrate-Co-3-Hydroxyvalerate) Derived From Fruit Pulp Biowaste. *Front. Sustain. Food Syst.* **2018**, *2*, 38. [CrossRef]
35. Koutsoumanis, K.; Alvarez-Ordóñez, A.; Bolton, D.; Bover-Cid, S.; Chemaly, M.; Davies, R.; De Cesare, A.; Herman, L.; Hilbert, F.; Lindqvist, R.; et al. The Efficacy and Safety of High-Pressure Processing of Food. *EFSA J.* **2022**, *20*, e07128. [CrossRef]
36. Iqbal, A.; Murtaza, A.; Pinto, C.A.; Saraiva, J.A.; Liu, X.; Zhu, Z. High-Pressure Processing for Food Preservation. In *Innovative and Emerging Technologies in the Bio-Marine Food Sector-Applications, Regulations, and Prospects*; Garcia-Vaquero, M., Rajauria, G., Eds.; Academic Press: Cambridge, MA, USA, 2022; pp. 495–518. ISBN 9780128200964.
37. Ravichandran, C.; Jayachandran, L.E.; Kothakota, A.; Pandiselvam, R.; Balasubramaniam, V.M. Influence of High Pressure Pasteurization on Nutritional, Functional and Rheological Characteristics of Fruit and Vegetable Juices and Purees-an Updated Review. *Food Control* **2023**, *146*, 109516. [CrossRef]
38. Machado, F.; Duarte, R.V.; Pinto, C.A.; Casal, S.; Lopes-da-Silva, J.A.; Saraiva, J.A. High Pressure and Pasteurization Effects on Dairy Cream. *Foods* **2023**, *12*, 3640. [CrossRef] [PubMed]
39. Scepankova, H.; Majtan, J.; Estevinho, L.M.; Saraiva, J.A. The High Pressure Preservation of Honey: A Comparative Study on Quality Changes during Storage. *Foods* **2024**, *13*, 989. [CrossRef] [PubMed]
40. *ASTM D882-18*; Standard Test Method For Tensile Properties of Thin Plastic Sheeting. ASTM International: West Conshohocken, PA, USA, 2018.
41. *ASTM E96/E96M-15*; Standard Test Methods for Water Vapor Transmission of Materials. ASTM International: West Conshohocken, PA, USA, 2016.
42. de Farias, P.M.; Barros de Vasconcelos, L.; da Silva Ferreira, M.E.; Alves Filho, E.G.; De Freitas, V.A.A.; Tapia-Blácido, D.R. Nopal Cladode as a Novel Reinforcing and Antioxidant Agent for Starch-Based Films: A Comparison with Lignin and Propolis Extract. *Int. J. Biol. Macromol.* **2021**, *183*, 614–626. [CrossRef] [PubMed]
43. *ASTM E2550-21*; Standard Test Method for Thermal Stability by Thermogravimetry. ASTM International: West Conshohocken, PA, USA, 2021.
44. Liu, Y.; Liang, X.; Wang, S.; Qin, W.; Zhang, Q. Electrospun Antimicrobial Polylactic Acid/Tea Polyphenol Nanofibers For. *Polymers* **2018**, *10*, 561. [CrossRef] [PubMed]
45. Chen, Z.; Guan, M.; Bian, Y.; Yin, X. Multifunctional Electrospun Nanofibers for Biosensing and Biomedical Engineering Applications. *Biosensors* **2024**, *14*, 13. [CrossRef]
46. Chew, S.Y.; Wen, Y.; Dzenis, Y.; Leong, K.W. The Role of Electrospinning in the Emerging Field of Nanomedicine. *Curr. Pharm. Des.* **2006**, *12*, 4751–4770. [CrossRef]
47. Badmus, M.; Liu, J.; Wang, N.; Radacsi, N.; Zhao, Y. Nano Materials Science Hierarchically Electrospun Nano Fi Bers and Their Applications: A Review. *Nano Mater. Sci.* **2021**, *3*, 213–232. [CrossRef]
48. Wannatong, L.; Sirivat, A.; Supaphol, P. Effects of Solvents on Electrospun Polymeric Fibers: Preliminary Study on Polystyrene. *Polym. Sci.* **2004**, *1859*, 1851–1859. [CrossRef]
49. Sun, L.; Sun, J.; Chen, L.; Niu, P.; Yang, X.; Guo, Y. Preparation and Characterization of Chitosan Film Incorporated with Thinned Young Apple Polyphenols as an Active Packaging Material. *Carbohydr. Polym.* **2017**, *163*, 81–91. [CrossRef]
50. Xiao, Y.; Luo, H.; Tang, R.; Hou, J. Preparation and Applications of Electrospun Optically Transparent Fibrous Membrane. *Polymers* **2021**, *13*, 506. [CrossRef] [PubMed]
51. Stoll, L.; Domenek, S.; Flôres, S.H.; Marli, S.; Alessandro, B.N.; Rios, D.O. Polylactide Films Produced with Bixin and Acetyl Tributyl Citrate: Functional Properties for Active Packaging. *J. Appl. Polym. Sci.* **2020**, *138*, 50302. [CrossRef]
52. Farah, S.; Anderson, D.G.; Langer, R. Physical and Mechanical Properties of PLA, and Their Functions in Widespread Applications—A Comprehensive Review. *Adv. Drug Deliv. Rev.* **2016**, *107*, 367–392. [CrossRef] [PubMed]
53. Burg, K.J.L.; Holder, W.D.; Culberson, C.R.; Beiler, R.J.; Greene, K.G.; Loebsack, A.B.; Roland, W.D.; Mooney, D.J.; Halberstadt, C.R. Parameters Affecting Cellular Adhesion to Polylactide Films. *J. Biomater. Sci. Polym. Ed.* **1999**, *10*, 147–161. [CrossRef]
54. Murariu, M.; Dubois, P. PLA Composites: From Production to Properties. *Adv. Drug Deliv. Rev.* **2016**, *107*, 17–46. [CrossRef]
55. Meng, X.; Bocharova, V.; Tekinalp, H.; Cheng, S.; Kisliuk, A.; Sokolov, A.P.; Kunc, V.; Peter, W.H.; Ozcan, S. Toughening of Nanocelluose/PLA Composites via Bio-Epoxy Interaction: Mechanistic Study. *Mater. Des.* **2018**, *139*, 188–197. [CrossRef]
56. Bin Rashid, A.; Haque, M.; Islam, S.M.M.; Uddin Labib, K.M.R. Nanotechnology-Enhanced Fiber-Reinforced Polymer Composites: Recent Advancements on Processing Techniques and Applications. *Heliyon* **2024**, *10*, e24692. [CrossRef]
57. Jamróz, E.; Kulawik, P.; Kopel, P. The Effect of Nanofillers on the Functional Properties of Biopolymer-Based Films: A Review. *Polymers* **2019**, *11*, 675. [CrossRef]
58. Trivedi, A.K.; Gupta, M.K. PLA Based Biodegradable Bionanocomposite Filaments Reinforced with Nanocellulose: Development and Analysis of Properties. *Sci. Rep.* **2024**, *14*, 23819. [CrossRef]
59. Mazaheri, M.; Kim, J.T.; Shin, G.H. Synergistic Enhancement of PLA/PHA Bio-Based Films Using Tempo-Oxidized Cellulose Nanofibers, Graphene Oxide, and Clove Oil for Sustainable Packaging. *Mater. Today Commun.* **2025**, *42*, 111531. [CrossRef]

60. Guo, M.; Duan, Y.; Li, Z.; Liu, R.; Qin, C.; Li, Q. Role of Silane Compatibilization on Cellulose Nanofiber Reinforced Poly (Lactic Acid) (PLA) Composites with Superior Mechanical Properties, Thermal Stability, and Tunable Degradation Rates. *Int. J. Biol. Macromol.* **2025**, *297*, 139836. [CrossRef] [PubMed]
61. Cacciotti, I.; Fortunati, E.; Puglia, D.; Kenny, J.M.; Nanni, F. Effect of Silver Nanoparticles and Cellulose Nanocrystals on Electrospun Poly(Lactic) Acid Mats: Morphology, Thermal Properties and Mechanical Behavior. *Carbohydr. Polym.* **2014**, *103*, 22–31. [CrossRef] [PubMed]
62. Jonoobi, M.; Harun, J.; Mathew, A.P.; Oksman, K. Mechanical Properties of Cellulose Nanofiber (CNF) Reinforced Polylactic Acid (PLA) Prepared by Twin Screw Extrusion. *Compos. Sci. Technol.* **2010**, *70*, 1742–1747. [CrossRef]
63. Xu, P.P.; Yang, S.; Gao, X.R.; Chen, S.P.; Xu, L.; Zhong, G.J.; Huang, H.D.; Li, Z.M. Constructing Robust Chain Entanglement Network, Well-Defined Nanosized Crystals and Highly Aligned Graphene Oxide Nanosheets: Towards Strong, Ductile and High Barrier Poly(Lactic Acid) Nanocomposite Films for Green Packaging. *Compos. B Eng.* **2021**, *222*, 109048. [CrossRef]
64. Weng, Q.H.; Hu, M.H.; Wang, J.F.; Hu, J.J. Enhancing the Flexibility and Hydrophilicity of PLA via Polymer Blends: Electrospinning vs. Solvent Casting. *Polymers* **2025**, *17*, 800. [CrossRef]
65. Iwatake, A.; Nogi, M.; Yano, H. Cellulose Nanofiber-Reinforced Polylactic Acid. *Compos. Sci. Technol.* **2008**, *68*, 2103–2106. [CrossRef]
66. Islam, M.S.; Ang, B.C.; Andriyana, A.; Afifi, A.M. A Review on Fabrication of Nanofibers via Electrospinning and Their Applications. *SN Appl. Sci.* **2019**, *1*, 1248. [CrossRef]
67. Morel, A.; Domaschke, S.; Urundolil Kumaran, V.; Alexeev, D.; Sadeghpour, A.; Ramakrishna, S.N.; Ferguson, S.J.; Rossi, R.M.; Mazza, E.; Ehret, A.E.; et al. Correlating Diameter, Mechanical and Structural Properties of Poly(L-Lactide) Fibres from Needleless Electrospinning. *Acta Biomater.* **2018**, *81*, 169–183. [CrossRef]
68. Guivier, M.; Chevigny, C.; Domenek, S.; Casalinho, J.; Perré, P.; Almeida, G. Water Vapor Transport Properties of Bio-Based Multilayer Materials Determined by Original and Complementary Methods. *Sci. Rep.* **2024**, *14*, 50. [CrossRef]
69. Wang, J.; Gardner, D.J.; Stark, N.M.; Bousfield, D.W.; Tajvidi, M.; Cai, Z. Moisture and Oxygen Barrier Properties of Cellulose Nanomaterial-Based Films. *ACS Sustain. Chem. Eng.* **2018**, *6*, 49–70. [CrossRef]
70. Oesef, K.; Cranston, E.D.; Abdin, Y. Current Advances in Processing and Modification of Cellulose Nanofibrils for High-Performance Composite Applications. *Mater. Des.* **2024**, *247*, 113417. [CrossRef]
71. Solhi, L.; Guccini, V.; Heise, K.; Solala, I.; Niinivaara, E.; Xu, W.; Mihhels, K.; Kröger, M.; Meng, Z.; Wohlert, J.; et al. Understanding Nanocellulose-Water Interactions: Turning a Detriment into an Asset. *Chem. Rev.* **2023**, *123*, 1925–2015. [CrossRef] [PubMed]
72. Esakkimuthu, E.S.; Ponnuchamy, V.; Sipponen, M.H.; DeVallance, D. Elucidating Intermolecular Forces to Improve Compatibility of Kraft Lignin in Poly(Lactic Acid). *Front. Chem.* **2024**, *12*, 1347147. [CrossRef] [PubMed]
73. Bikiaris, N.D.; Koumentakou, I.; Samiotaki, C.; Meimaroglou, D.; Varytimidou, D.; Karatza, A.; Kalantzis, Z.; Roussou, M.; Bikiaris, R.D.; Papageorgiou, G.Z. Recent Advances in the Investigation of Poly(Lactic Acid) (PLA) Nanocomposites: Incorporation of Various Nanofillers and Their Properties and Applications. *Polymers* **2023**, *15*, 1196. [CrossRef] [PubMed]
74. Keeratipinit, K.; Wijaranakul, P.; Wanmolee, W.; Hararak, B. Preparation of High-Toughness Cellulose Nanofiber/Polylactic Acid Bionanocomposite Films via Gel-like Cellulose Nanofibers. *ACS Omega* **2024**, *9*, 26159–26167. [CrossRef]
75. Forti, E.S.; El Awad Azrak, S.M.; Ng, X.Y.; Cho, W.; Schueneman, G.T.; Moon, R.J.; Fox, D.M.; Youngblood, J.P. Mechanical Enhancement of Cellulose Nanofibril (CNF) Films through the Addition of Water-Soluble Polymers. *Cellulose* **2021**, *28*, 6449–6465. [CrossRef]
76. Saeb, M.R.; Ramezani-Dakhel, H.; Khonakdar, H.A.; Heinrich, G.; Wagenknecht, U. A Comparative Study on Curing Characteristics and Thermomechanical Properties of Elastomeric Nanocomposites: The Effects of Eggshell and Calcium Carbonate Nanofillers. *J. Appl. Polym. Sci.* **2013**, *127*, 4241–4250. [CrossRef]
77. Abdullah, J.A.A.; Benítez, J.J.; Guerrero, A.; Romero, A. Sustainable Integration of Zinc Oxide Nanoparticles: Enhancing Properties of Poly(ε-Caprolactone) Electrospun Nanofibers and Cast Films. *Coatings* **2023**, *13*, 1665. [CrossRef]
78. Shankar, S.; Wang, L.F.; Rhim, J.W. Effect of Melanin Nanoparticles on the Mechanical, Water Vapor Barrier, and Antioxidant Properties of Gelatin-Based Films for Food Packaging Application. *Food Packag. Shelf Life* **2019**, *21*, 100363. [CrossRef]
79. Spatafora Salazar, A.S.; Sáenz Cavazos, P.A.; Mújica Paz, H.; Valdez Fragoso, A. External Factors and Nanoparticles Effect on Water Vapor Permeability of Pectin-Based Films. *J. Food Eng.* **2019**, *245*, 73–79. [CrossRef]
80. Argel-Pérez, S.; Velásquez-Cock, J.; Zuluaga, R.; Gómez-Hoyos, C. Improving Hydrophobicity and Water Vapor Barrier Properties in Paper Using Cellulose Nanofiber-Stabilized Cocoa Butter and PLA Emulsions. *Coatings* **2024**, *14*, 1310. [CrossRef]
81. Deng, L.; Kang, X.; Liu, Y.; Feng, F.; Zhang, H. Characterization of Gelatin/Zein Films Fabricated by Electrospinning vs Solvent Casting. *Food Hydrocoll.* **2018**, *74*, 324–332. [CrossRef]
82. Costa, S.M.; Ferreira, D.P.; Teixeira, P.; Ballesteros, L.F.; Teixeira, J.A.; Fangueiro, R. Active Natural-Based Films for Food Packaging Applications: The Combined Effect of Chitosan and Nanocellulose. *Int. J. Biol. Macromol.* **2021**, *177*, 241–251. [CrossRef] [PubMed]
83. Zhang, Y.; Liu, C.; Wu, M.; Li, Z.; Li, B. Impact of the Incorporation of Nano-Sized Cellulose Formate on the End Quality of Polylactic Acid Composite Film. *Nanomaterials* **2022**, *12*, 1. [CrossRef] [PubMed]

84. Wang, C.; Wang, J.; Zeng, L.; Qiao, Z.; Liu, X.; Liu, H.; Zhang, J.; Ding, J. Fabrication of Electrospun Polymer Nanofibers with Diverse Morphologies. *Molecules* **2019**, *24*, 834. [CrossRef] [PubMed]
85. Zhang, L.; Ye, Z.; Hou, P. Biodegradable PLA/TPU Blends with Improved Mechanical Properties. *Mater. Lett.* **2025**, *387*, 138205. [CrossRef]
86. Hussain, M.; Khan, S.M.; Shafiq, M.; Al-Dossari, M.; Alqsair, U.F.; Khan, S.U.; Khan, M.I. Comparative Study of PLA Composites Reinforced with Graphene Nanoplatelets, Graphene Oxides, and Carbon Nanotubes: Mechanical and Degradation Evaluation. *Energy* **2024**, *308*, 132917. [CrossRef]
87. Khan, A.; Sapuan, S.M.; Zainudin, E.S.; Zuhri, M.Y.M. Physical, Mechanical and Thermal Properties of Novel Bamboo/Kenaf Fiber-Reinforced Polylactic Acid (PLA) Hybrid Composites. *Compos. Commun.* **2024**, *51*, 102103. [CrossRef]
88. Scaffaro, R.; Lopresti, F. Properties-Morphology Relationships in Electrospun Mats Based on Polylactic Acid and Graphene Nanoplatelets. *Compos. Part A Appl. Sci. Manuf.* **2018**, *108*, 23–29. [CrossRef]
89. Li, F.J.; Yu, X.T.; Huang, Z.; Liu, D.F. Interfacial Improvements in Cellulose Nanofibers Reinforced Polylactide Bionanocomposites Prepared by in Situ Reactive Extrusion. *Polym. Adv. Technol.* **2021**, *32*, 2352–2366. [CrossRef]
90. Huan, S.; Liu, G.; Cheng, W.; Han, G.; Bai, L. Electrospun Poly(Lactic Acid)-Based Fibrous Nanocomposite Reinforced by Cellulose Nanocrystals: Impact of Fiber Uniaxial Alignment on Microstructure and Mechanical Properties. *Biomacromolecules* **2018**, *19*, 1037–1046. [CrossRef] [PubMed]
91. Fortunati, E.; Peltzer, M.; Armentano, I.; Torre, L.; Jiménez, A.; Kenny, J.M. Effects of Modified Cellulose Nanocrystals on the Barrier and Migration Properties of PLA Nano-Biocomposites. *Carbohydr. Polym.* **2012**, *90*, 948–956. [CrossRef] [PubMed]
92. Lafia-Araga, R.A.; Sabo, R.; Nabinejad, O.; Matuana, L.; Stark, N. Influence of Lactic Acid Surface Modification of Cellulose Nanofibrils on the Properties of Cellulose Nanofibril Films and Cellulose Nanofibril–Poly (Lactic Acid) Composites. *Biomolecules* **2021**, *11*, 1346. [CrossRef] [PubMed]
93. Abera, G. Review on High-Pressure Processing of Foods. *Cogent. Food Agric.* **2019**, *5*, 1568725. [CrossRef]
94. Muntean, M.-V.; Marian, O.; Barbieru, V.; Cătunescu, G.M.; Ranta, O.; Drocas, I.; Terhes, S. High Pressure Processing in Food Industry–Characteristics and Applications. *Agric. Agric. Sci. Procedia* **2016**, *10*, 377–383. [CrossRef]
95. Aganovic, K.; Hertel, C.; Vogel, R.F.; Johne, R.; Schlüter, O.; Schwarzenbolz, U.; Jäger, H.; Holzhauser, T.; Bergmair, J.; Roth, A.; et al. Aspects of High Hydrostatic Pressure Food Processing: Perspectives on Technology and Food Safety. *Compr. Rev. Food Sci. Food Saf.* **2021**, *20*, 3225–3266. [CrossRef] [PubMed]
96. López-Rubio, A.; Lagarón, J.M.; Hernández-Muñoz, P.; Almenar, E.; Catalá, R.; Gavara, R.; Pascall, M.A. Effect of High Pressure Treatments on the Properties of EVOH-Based Food Packaging Materials. *Innov. Food Sci. Emerg. Technol.* **2005**, *6*, 51–58. [CrossRef]
97. Muller, J.; González-Martínez, C.; Chiralt, A. Combination Of Poly(Lactic) Acid and Starch for Biodegradable Food Packaging. *Materials* **2017**, *10*, 952. [CrossRef]
98. Lavoine, N.; Desloges, I.; Dufresne, A.; Bras, J. Microfibrillated Cellulose-Its Barrier Properties and Applications in Cellulosic Materials: A Review. *Carbohydr. Polym.* **2012**, *90*, 735–764. [CrossRef]
99. Abdulkhani, A.; Hosseinzadeh, J.; Ashori, A.; Dadashi, S. Preparation and Characterization of Modified Celllose Nanofibers Reinforced Polylactic Acid Nanocomposite. *Polym. Test.* **2014**, *35*, 73–79. [CrossRef]
100. Barreira, L.; Resek, E.; Rodrigues, M.J.; Rocha, M.I.; Pereira, H.; Bandarra, N.; da Silva, M.M.; Varela, J.; Custódio, L. Halophytes: Gourmet Food with Nutritional Health Benefits? *J. Food Comp. Anal.* **2017**, *59*, 35–42. [CrossRef]
101. Lima, A.R.; Castañeda-Loaiza, V.; Salazar, M.; Nunes, C.; Quintas, C.; Gama, F.; Pestana, M.; Correia, P.J.; Santos, T.; Varela, J.; et al. Influence of Cultivation Salinity in the Nutritional Composition, Antioxidant Capacity and Microbial Quality of Salicornia Ramosissima Commercially Produced in Soilless Systems. *Food. Chem.* **2020**, *333*, 127525. [CrossRef]